


Cite this: *Analyst*, 2024, **149**, 5739

# Phenoxy-1,2-dioxetane-based activatable chemiluminescent probes: tuning of photophysical properties for tracing enzymatic activities in living cells

Jagpreet Singh Sidhu,<sup>a</sup> Gurjot Kaur,<sup>b</sup> Atharva Rajesh Chavan,<sup>a</sup> Mandeep K. Chahal<sup>c</sup> and Rajeev Taliyan<sup>a</sup>

The use of chemiluminophores for tracing enzymatic activities in live-cell imaging has gained significant attention, making them valuable tools for diagnostic applications. Among various chemiluminophores, the phenoxy-1,2-dioxetane scaffold exhibits significant structural versatility and its activation is governed by the chemically initiated electron exchange luminescence (CIEEL) mechanism. This mechanism can be initiated by enzymatic activity, changes in pH, or other chemical stimuli. The photophysical properties of phenoxy-1,2-dioxetanes can be fine-tuned through the incorporation of different substituents on the phenolic ring and by anchoring them with specific triggers. This review discusses the variations in physicochemical properties, including emission maxima, quantum yield, aqueous solubility, and  $pK_a$ , as influenced by structural modifications, thereby establishing a comprehensive structure–activity relationship. Furthermore, it categorises the probes based on different enzyme classes, such as hydrolase-sensitive probes, oxidoreductase-responsive probes, and transferase-activatable phenoxy-1,2-dioxetanes, offering a promising platform technology for the early diagnosis of diseases and disorders. The summary section highlights key opportunities and limitations associated with applying phenoxy-1,2-dioxetanes in achieving precise and effective enzyme assays.

Received 10th August 2024,  
Accepted 1st November 2024

DOI: 10.1039/d4an01082e

rscl.li/analyst

## 1 Introduction

Activatable sensing systems have become increasingly prevalent in medical science to trace diverse bioinformatics in the context of location, time, and environment in living subjects.<sup>1</sup> Such systems are sensitive to external stimuli such as enzymes, biomolecules, or other cellular events and give the readout signal.<sup>2</sup> The “always on” sensing probes display unchanging optical signals in the presence or absence of target species and suffer from high background signals. In contrast, an activatable probe changes its output signal once it comes into contact with the target of interest and thus provides a better signal-to-background ratio.<sup>3,4</sup> Optically detected chemical probes emerge as promising candidates for sensing and diagnosis due to their advantages, including high specificity, low detection thresholds, rapid response times, and straightforward technical implementation.<sup>5,6</sup> The last decade has witnessed

significant progress in cellular imaging techniques to reveal living-cell secrets and disclose undiscovered disease information.<sup>7,8</sup> However, high energy from excitation sources causes permanent damage to living tissues, while low signal-to-noise ratios and autofluorescence backgrounds limit the applications of fluorescence-based sensors in clinical samples.<sup>9,10</sup> Moreover, the inadequate penetration of light into deep biological tissues primarily caused by scattering and absorption of high energy short waves is also a serious concern.<sup>11,12</sup> Unlike fluorescence, chemiluminescence is an optical imaging technique in which a luminophore generates light without requiring excitation energy from an external source.<sup>13,14</sup> It is a chemical reaction-based light emission phenomenon that can occur in a wide range of chemical events even inside living systems, where excited-state intermediates subsequently break down to release the energy in the form of visible light.<sup>15,16</sup> The unique feature of chemiluminescence results in exceptional sensitivity by eliminating the need for excitation energy/source.<sup>17</sup> As a result, it can mitigate the photobleaching, light scattering, background disturbance, and autofluorescence of biomolecules.<sup>18,19</sup> Thus, chemiluminescent probes have been actively explored for the non-invasive imaging of cellular events in living cells. Leveraging the poten-

<sup>a</sup>Department of Pharmacy, Birla Institute of Technology and Science Pilani, Pilani Campus, Rajasthan, 333031, India. E-mail: jagpreet.sidhu@pilani.bits-pilani.ac.in

<sup>b</sup>Khalsa College Amritsar, Punjab, 143002, India

<sup>c</sup>School of Chemistry and Forensic Science, University of Kent, Canterbury, CT2 7NH, UK

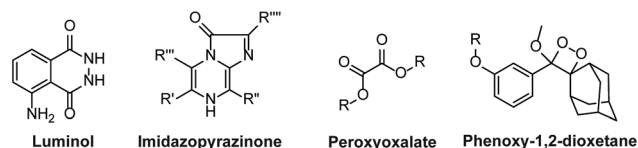



Fig. 1 Chemical scaffolds of chemiluminescence probes.

tial of chemiluminescence, innovative imaging, and therapeutic approaches continues to emerge, necessitating a comprehensive and current assessment of advancements within this dynamic research domain.

The majority of these chemiluminescent probes are categorized into four groups:<sup>20</sup> 1. luminol and its derivatives, 2. cypridina luciferin derivatives, 3. peroxyoxalate esters, and 4. Phenoxy-1,2-dioxetanes (Fig. 1). The luminescence of luminol and peroxyoxalate derivatives is generally triggered by oxidizing agents.<sup>21,22</sup> In such cases, the probe undergoes oxidation, forming a highly energetic and unstable intermediate. Subsequently, the intermediate decomposes to generate luminogenic species that emit photons as it returns to its ground state.<sup>23,24</sup> These probes are commonly used for imaging hydrogen peroxide ( $H_2O_2$ ) because it serves both as an oxidizing agent and as a target analyte in numerous research studies.<sup>25,26</sup> Furthermore, cypridina-based chemiluminescent probes have been reported to be activated in the presence of singlet oxygen species.<sup>27</sup> As a result, most cypridina-based and luminol-based probes have been developed to trace cellular events linked to oxidizing species.<sup>28</sup> However, it is crucial to note that in addition to these analytes, enzymes play an extremely significant role in nearly every cellular pathway. Enzymes are ubiquitous polypeptide biomolecules that catalyse selective and specific biochemical reactions.<sup>29,30</sup> A diverse array of enzymes, including esterases, oxidases, reductases, proteases,

and transferases are key biocatalysts and central figures in the chemistry of living organisms. Their involvement ranges from facilitating abnormal cellular growth to triggering inflammatory responses to a diseased state.<sup>31,32</sup> Therefore, understanding the physiology of enzymes in disease pathogenesis offers invaluable insights for developing targeted therapeutic interventions and diagnostics. The diagnosis of disease using enzyme-triggering motifs provides a promising approach to designing activatable probes. Presently, a plethora of enzyme-activatable optical probes has been documented.<sup>33</sup> In this regard, the luminescence properties of phenoxy-1,2-dioxetanes have been widely explored in the literature to facilitate the tracing of enzymatic activities.<sup>34,35</sup> Its luminescence properties can be tailored as per the specific enzyme's catalytic nature. Unlike other chemiluminophores, phenoxy-1,2-dioxetanes can be modified so that they become directly activated by the biochemical reactions of the enzymes without any assistance from oxidizing species.<sup>36–38</sup> Interestingly, their emission has been controlled by shielding of the phenolate with a protecting group, which can be only activated in an enzymatic event, therefore spontaneously initiating chemiluminescence.<sup>39</sup> For several decades, triggerable dioxetanes of this kind have been employed in commercially available *in vitro* assays. Recently, there has been a huge surge of research interest in the utilisation of chemiluminescent phenoxy-1,2-dioxetanes for *in vivo* imaging, mainly due to their biocompatibility and potential to emit sufficiently bright light essential for live animal imaging.<sup>40–43</sup>

Over the last decade, the structural properties of phenoxy-1,2-dioxetanes have been extensively explored through derivatisation with various functional groups. These structural changes result in fast chemo-excitation,  $pK_a$  adjustment, improved quantum yields, and emission enhancement in physiological buffers.<sup>44,45</sup> As such, this review summarises the



Jagpreet Singh Sidhu

Dr Jagpreet Sidhu is an Assistant Professor at Birla Institute of Technology and Science (BITS) Pilani, Pilani Campus in the Pharmacy Department. He received his PhD from IIT Ropar, India in 2020. During his doctoral program, he specialized in the development of activatable fluorogenic probes tailored for disease diagnostic applications. During his postdoctoral program at IISc Bangalore, he worked on the synthesis of optical reporters

for tracing enzymatic activity in living cells. He also worked on the synthesis of deuterated synthetic fatty acids to establish the catalytic mechanism of membrane-bound enzymes. He developed interdisciplinary approaches that integrate organic synthesis, chemical biology, protein engineering, and biochemical analysis.



Mandeep K. Chahal

Dr Mandeep K. Chahal completed her PhD at the IIT Roorkee, India, in 2017, working on the synthetic chemistry of substituted porphyrins and their applications in sensing. Further on, she worked as a post-doctoral research fellow with Dr Jonathan P. Hill, Prof. Katsuhiko Ariga and Dr Shinsuke Ishihara at the National Institute for Materials Science (NIMS), Japan. She moved to the University of Southampton, in the UK, where

she completed a Royal Society Newton International Fellowship working with Prof. Steve Goldup on mechanically interlocked molecules (MIMs). From 2023, she has been working as a Lecturer at the University of Kent; here, she is exploring diverse applications in the functionalisation of tetrapyrrole macrocycles.



recent advancements in phenoxy-1,2-dioxetane derivatives tailored for monitoring enzymatic activities. It also explores the impact of different functional groups on their photophysical properties including emission maxima, quantum yields, and further outlines the designing principles of corresponding systems. Additionally, the review discusses potential challenges and outlines future directions for developing chemiluminescent technologies.

## 2 Photophysical and structural properties of phenoxy-1,2-dioxetanes

Over the years, phenoxy-1,2-dioxetanes have emerged as powerful light-emitting probes for bio-imaging applications, especially for activatable sensing.<sup>46</sup> The key advancement in the chemistry of these compounds occurred approximately three decades ago, marked by the Schaap group's discovery of triggerable dioxetanes.<sup>36,37</sup> Initial investigations revealed the involvement of phenoxy-1,2-dioxetane as an inherently unstable intermediate in numerous chemiluminescent systems.<sup>47</sup> Over time, certain phenoxy-1,2-dioxetanes were developed that can be selectively activated by a specific analyte of interest, which results in chemiluminescence.<sup>41,48,49</sup> The activation of the 1,2-dioxetane probe occurs *via* the chemically initiated electron exchange luminescence (CIEEL) mechanism, where chemiexcitation is initiated through phenolate-dioxetane biradical intermediates (Fig. 2). These biradical intermediates undergo further decomposition through the intramolecular back electron transfer (BET) mechanism and release energy to excite a benzoate ester. Ultimately, it returns to the ground state and emits light of a specific wavelength.<sup>18,50–54</sup> Unlike conventional chemiluminophores, the chemiexcitation processes of phenoxy-1,2-dioxetanes rely not only on oxidative species, but can also have chemiluminescence triggered by enzymes.<sup>19,55</sup>

However, to activate first-generation phenoxy-1,2-dioxetanes for chemiluminescence, a higher pH value (approximately 10) was required, which hampered their applications for live animal imaging.<sup>56</sup> Hence, to decrease the  $pK_a$  of phenol-diox-

tane, Lippert and coworkers synthesised both halogenated and unsubstituted derivatives of phenoxy-1,2-dioxetane (**CL-1a**, **CL-1b**, and **CL-1c**).<sup>41</sup> This work revealed that the acidity of phenol is increased due to the presence of *ortho* halogens and resulted in the highest chemiluminescence at pH 7.4, therefore confirming that lowering the  $pK_a$  of phenol is accountable for enhancing chemiluminescence at physiological pH (Fig. 3). Furthermore, to improve the chemiluminescence in an aqueous medium at neutral pH, Higuchi and coworkers introduced an acetamide group *ortho* to phenol (**CL-2**).<sup>57</sup> **CL-2** is expected to have a lower  $pK_a$  value due to intramolecular  $NH\cdots O$  hydrogen bonding interactions in both neutral and anionic states. Recently, Pu and coworkers reported benzoxazole-substituted phenoxy-1,2-dioxetane probes (**CL-3a** and **CL-3b**), to study the role of intramolecular hydrogen bonding in their chemiluminescence response.<sup>58</sup> They have found that the presence of the benzoxazole moiety resulted in both increased chemiluminescence half-lives (up to ~33-fold) and 8.2-fold greater brightness in comparison to the classical methylacrylate-phenoxy-1,2-dioxetane derivative (**CL-4**) in aqueous solution. Although halogens and H-bonding groups containing probes were activatable at physiological pH in aqueous solution, their chemiluminescence quantum yields were not improved significantly due to the quenching effect of water molecules. Shabat and coworkers have adopted multiple strategies to improve aqueous emission and quantum yield. They hypothesised that enhancement in quantum yield of phenoxy-1,2-dioxetane could be achieved by incorporating an electron acceptor, namely an acrylic ester/acrylonitrile group *ortho* to the phenolate donor.<sup>59</sup> To investigate the role of electron-withdrawing groups (EWGs), they synthesised acryl-substituted phenoxy-benzoate derivatives, **CL-5** and **CL-6**.<sup>59</sup> The presence of EWGs significantly improved their emission in water, with  $\Phi_{CL}$  (chemiluminescence quantum yield) values reaching up to 40% (Table 1). These findings suggested that the introduction of an acryl group into the phenoxy-1,2-dioxetane could elevate its  $\Phi_{CL}$  under physiological conditions. Furthermore, replacing acryl ester and acrylonitrile with acrylic acid (**CL-5d**) substantially amplified the chemiexcitation rate in aqueous solution. Additionally, the presence of chlorine at the *ortho*

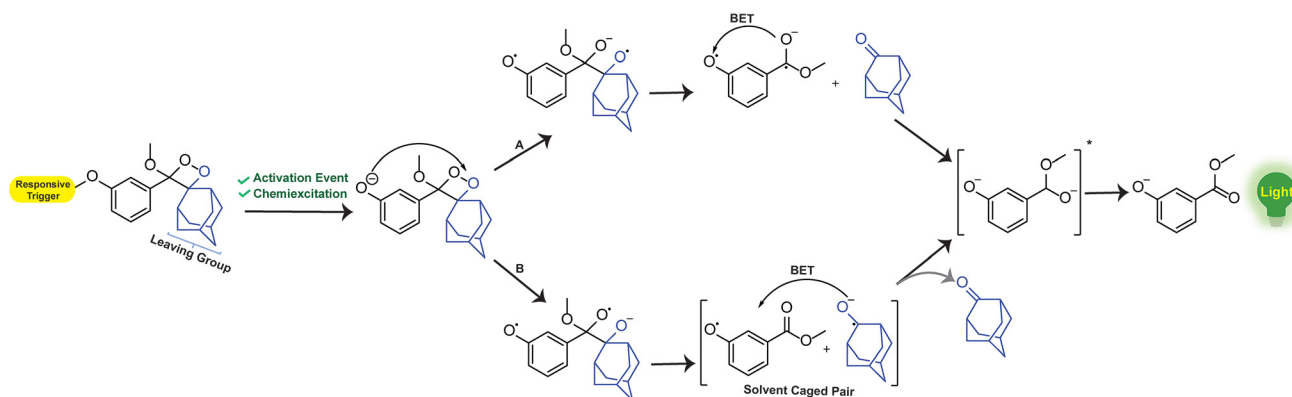


Fig. 2 Chemiexcitation activation mechanism of phenoxy-1,2-dioxetane-based probes through CIEEL.



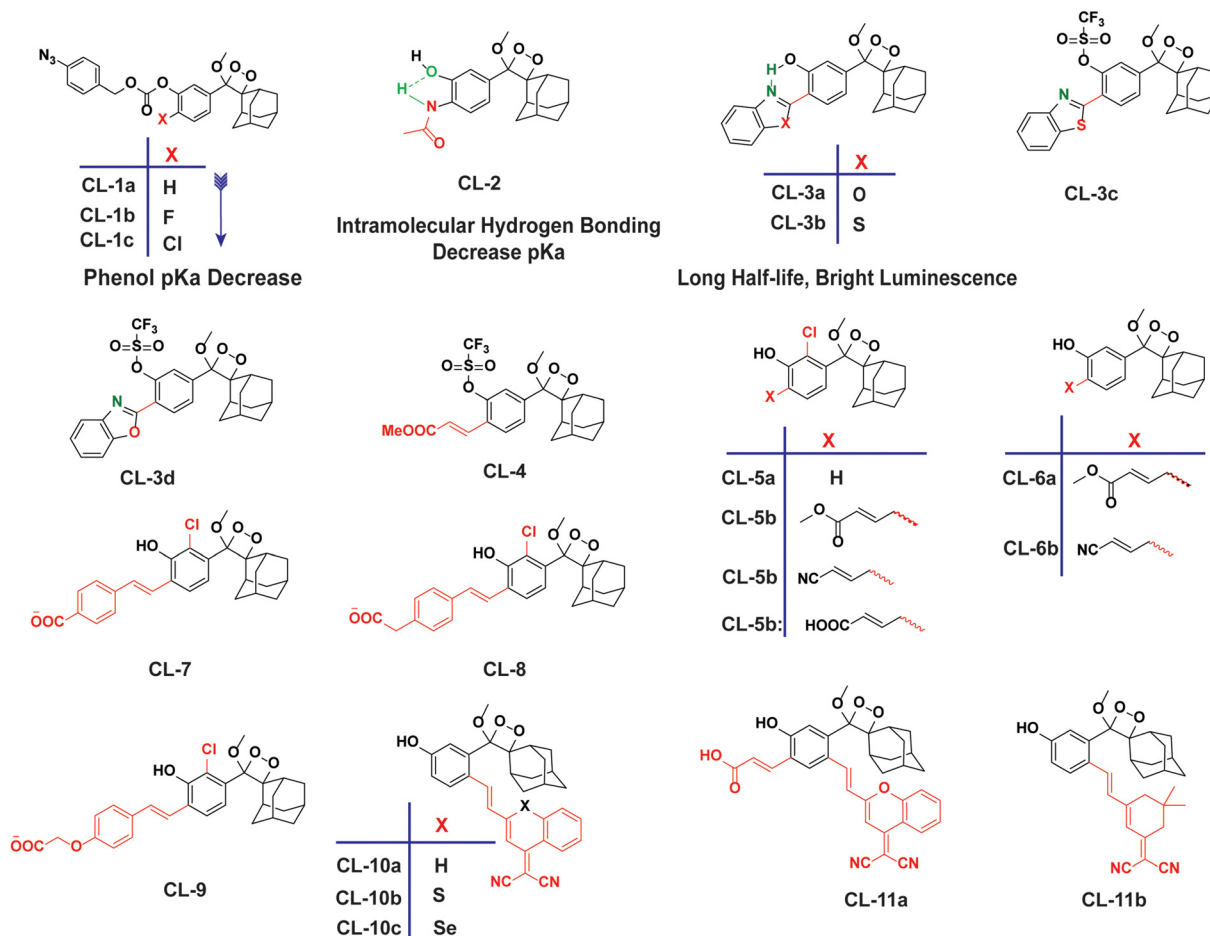


Fig. 3 Chemical structural frameworks of phenoxy-1,2-dioxetane derivatives (CL-1 to CL-11).

Table 1 Photo-physical properties of CL-2 to CL-11

| Probe  | $\lambda_{\max}$ CL (nm) | $T_{1/2}$ | $\Phi_{\text{CL}} (\times 10^{-2} \text{ Einstein per mol})$ | Test condition         | Ref. |
|--------|--------------------------|-----------|--|------------------------|------|
| CL-2   | 450                      | —         | $2.7 \times 10^{-4}$   | pH 11.0                | 57   |
| CL-3b  | 515                      | 23.2 h    | —  | PBS (10% DMSO)         | 58   |
| CL-3c  | 515                      | 121 min   | 0.189  | PBS (pH 7.4, 10% DMSO) | 58   |
| CL-3d  | 515                      | 129 min   | 0.137  | PBS (pH 7.4, 10% DMSO) | 58   |
| CL-4   | 515                      | 3.6 min   | 0.023  | PBS (pH 7.4, 10% DMSO) | 58   |
| CL-5a  | 470                      | 17 min    | 0.003  | PBS (pH 7.4, 5% DMSO)  | 11   |
| CL-5b  | 540                      | ~7 min    | 2.5  | PBS (pH 7.4, 5% DMSO)  | 11   |
| CL-5c  | 525                      | 10 min    | 9.8  | PBS (pH 7.4, 5% DMSO)  |      |
| CL-5d  | 510                      | 85 s      | 0.098  | In PBS (10% DMSO)      |      |
| CL-6a  | 540                      | 23 min    | 2.3  | PBS (pH 7.4, 5% DMSO)  |      |
| CL-6b  | 525                      | 22 min    | 7.4  | PBS (pH 7.4, 5% DMSO)  |      |
| CL-7   | 535                      | 8.4 s     | 4.2  | PBS (pH 7.4, 10% DMSO) | 60   |
| CL-8   | 500                      | 5.1 s     | 1.4  | PBS (pH 7.4, 10% DMSO) | 60   |
| CL-9   | 490                      | 3.2 s     | 0.6  | PBS (pH 7.4, 10% DMSO) | 60   |
| CL-10a | 660                      | 178 min   | 0.82   | PBS (pH 7.4, 10% FBS)  | 61   |
| CL-10b | 760                      | —         | 0.23   | PBS (pH 7.4, 1% DMSO)  | 62   |
| CL-10c | 780                      | —         | 0.12   | PBS (pH 7.4, 1% DMSO)  | 62   |
| CL-11a | 690                      | 53 min    | 1.125  | PBS (pH 7.4, 10% FBS)  | 61   |
| CL-11b | 650                      | 14 min    | 2.90   | PBS (10% DMSO)         | 63   |

position reduced the  $pK_a$  of the phenolic OH, resulting in an enhanced extinction coefficient. The increase in extinction coefficient was attributed to the higher concentration of phen-

oxide ions in an aqueous medium induced by the chlorine substituent. However, this alteration did not affect the emission wavelength and had a minor impact on the quantum





yield. The improvement in the kinetic profile of luminophores is generally accompanied by a decrease in  $t_{1/2}$  of luminophores (Table 1). In summary, the luminophores substituted with an acryl group (with or without chlorine) demonstrate notably intense chemiluminescent emission upon deprotonation at pH 7.4, with their  $\Phi_{\text{CL}}$  reaching up to 3000 times the value seen for the unmodified structures.

Furthermore, in specific chemiluminescence bioassays, the absolute quantum yield of a luminophore is not the primary factor determining the efficacy of a chemiluminescent probe. Instead, what matters significantly is the rate at which chemiexcitation occurs within the free phenolate-dioxetane. Luminophores exhibiting rapid chemiexcitation kinetics are highly sought after because they have the potential to enhance the sensitivity of chemiluminescent analytical bioassays. A faster release of photons leads to a higher signal-to-noise ratio within a shorter timeframe, ultimately resulting in improved sensitivity. To improve the chemiexcitation rate, Shabat and coworkers stabilised the phenoxy radical with styryl substituents (CL-7, CL-8, and CL-9).<sup>60</sup> The chemiexcitation of the styryl derivatives happened approximately two orders of magnitude higher than the chemiexcitation of CL-5 and CL-6, as well as the unsubstituted Schaap's dioxetane (CL-5a). Furthermore, the change in the pH did not affect the half-lives and thus proved that chemiexcitation is an intrinsic factor without any impact on  $pK_a$ . With these structural modifications, the physicochemical properties of phenoxy-1,2-dioxetane derivatives were improved to visualise enzymatic activities in living cells. So, by considering all these parameters, the probes have been tailored for the sensing of enzymes, as discussed in the next section.

To employ Schaap's dioxetanes for live-cell imaging, it is crucial to enhance aqueous solubility and adjust their light emission towards the near-infrared (NIR) region. NIR wavelengths are highly advantageous for live-cell imaging as they can penetrate deeply into tissues and encounter less scattering than light with shorter wavelengths.<sup>64,65</sup> In pursuit of live-cell imaging, Shabat and coworkers conjugated dicyanomethylene-4H-chromene (DCMC) at the *para* position of the phenol donor in a phenoxy-dioxetane probe (CL-10a) that resulted in NIR emission at 660 nm with comparative quantum yield.<sup>61</sup> A particularly remarkable luminophore possessing a DCMC acceptor along with an acrylic acid substituent at the *ortho* position of the phenol (CL-11a) exhibited a faster kinetics ( $t_{1/2}$  53 minutes) profile than CL-10a ( $t_{1/2}$  178 minutes). Faster kinetics is attributed to a lower  $pK_a$  value for phenol, which ultimately affects the generation of phenolate species. Additionally, substituting an oxygen atom with sulfur in the dicyanomethylene-4H-chromene ring (CL-10b) leads to improvement both in NIR emission (760 nm) and also chemiluminescence quantum yield (Table 1). Interestingly, the substitution of sulfur with selenium (CL-10c) further increased the emission wavelength (780 nm); however, it compromised the  $\Phi_{\text{CL}}$  value ( $0.12 \times 10^{-2}$  Einstein per mol). The increment in emission energy was explained based on a decrease in the energy gap between the ground state and the excited state of the molecule. Among the three heteroatoms, the inclusion of

sulfur resulted in the brightest chemiluminescence and the highest signal-to-background ratio (SBR), of approximately 415.1, being exhibited. Further, the conjugation of 2-(3,5,5-trimethylcyclohex-2-en-1-ylidene)malononitrile to phenoxy-1,2-dioxetane (CL-11b) compromised the emission wavelength (650 nm) but improved the  $\Phi_{\text{CL}}$  ( $4.6 \times 10^{-2}$  Einstein per mol) beyond that of CL-11a.<sup>63</sup> Thereby, it is worth playing around with extended  $\pi$ -conjugation in the molecular structure of phenoxy-1,2-dioxetanes for tuning the spectroscopic parameters. The chemiluminescence spectroscopic data of phenoxy-1,2-dioxetanes are summarised in Table 1. The molecular structures and chemiluminescence parameters of phenoxy-1,2-dioxetanes with different *ortho* substituents are summarised in Table 2. Based on the photophysical properties and the chemical nature of the chemiluminophores, the structure–activity relationship has been illustrated in Fig. 4.

### 3 Enzyme-triggered phenoxy-1,2-dioxetane

#### 3.1 Hydrolase-selective chemiluminescent probe

**Fibroblast activation protein-alpha (FAP $\alpha$ ).** FAP $\alpha$  (EC3.4.21. B28) is a transmembrane type II serine proteolytic enzyme that participates in the hydrolysis of peptide bonds and is involved in multiple pathogeneses, including cancer.<sup>66,67</sup> It possesses the capability to break down various components of the extracellular matrix (ECM) and has dipeptidyl peptidase (DPP) activity. Degradation of the ECM is a key component of the process influencing the growth, invasion, and metastasis of tumors. It is also implicated in the excessive growth observed at the boundaries of keloid wounds and contributes to the invasive nature of keloids.<sup>68,69</sup> Therefore, tracing of FAP $\alpha$  activity holds significant importance in disease diagnosis. Recently, Cao and coworkers developed the first phenoxy-1,2-dioxetane-based chemiluminescent probes (CL-12a, CL-12b, and CL-12c) bearing acrylic ester and chlorine groups *ortho* to the phenol for the detection of FAP $\alpha$ .<sup>70</sup> The phenolic OH was masked with glycine–proline dipeptide to restrain the chemiexcitation of the luminophore. FAP $\alpha$  hydrolysed the peptide bond after the proline, forming a phenoxy-dioxetane (through a rearrangement involving 1,6 elimination) that rapidly decomposes *via* the CIEEL process to an excited benzoate ester, which decayed to the ground state with the release of green light energy. The results suggested that probes exhibited highly selective and sensitive detection of FAP $\alpha$  with a limit of detection of 0.785, 0.965, and 0.587 ng mL<sup>-1</sup>, using CL-12a, CL-12b, and CL-12c, respectively. Among all the probes, CL-12a showed the highest selectivity with 33-fold and 121-fold emission enhancement toward FAP $\alpha$  over structurally similar enzymes, *i.e.* PREP (prolyl oligopeptidase) and DPPIV (dipeptidase IV), respectively, while CL-12b and CL-12c remained moderately to weakly selective, which might be due to the inappropriate interactions of the probe at the active pocket of the enzyme. Subsequently, the stronger chemiluminescence signal in the cytoplasm of CL-12a-treated HepG2



**Table 2** Spectroscopic parameters of phenoxy-1,2-dioxetane derivatives in PBS (100 mM), pH 7.4, 10% DMSO<sup>43</sup>

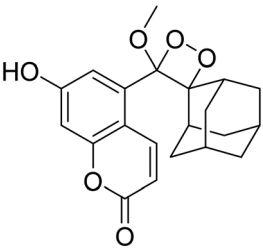
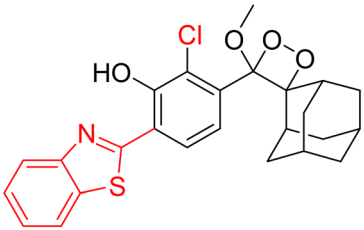
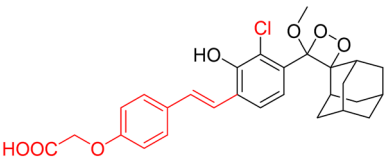
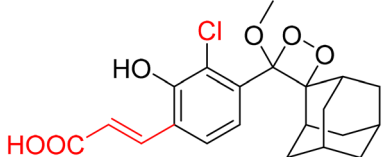
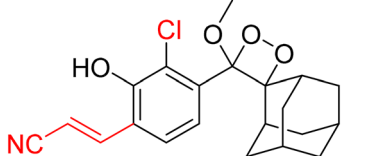
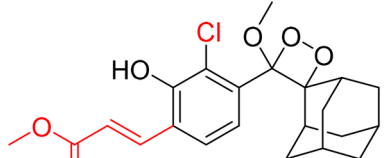
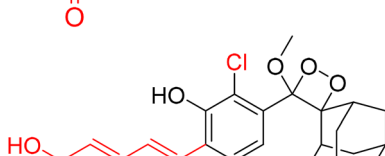
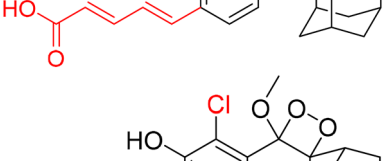
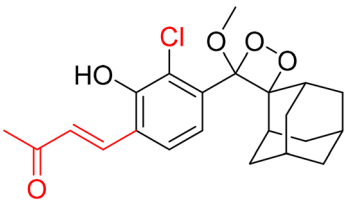
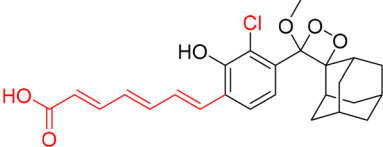
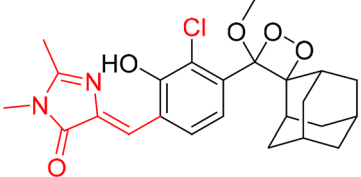
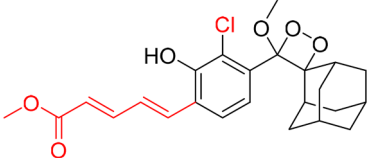
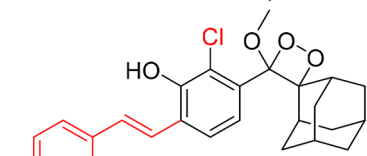
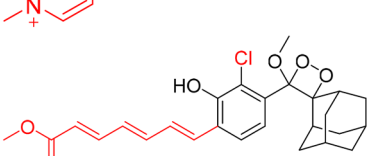
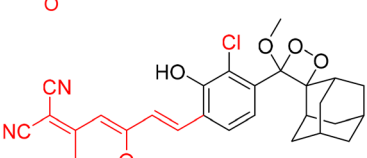
| Phenoxy-1,2-dioxetane   | $\lambda_{\text{max CL}}$ [nm] | $t_{1/2}$ | Relative brightness | $\Phi_{\text{CL}}$ % |
|---|--------------------------------|-----------|---------------------|----------------------|
|    | 460 nm                         | 16 h      | 1                   | 55                   |
|    | 490 nm                         | 10.3 h    | 0.70                | 20                   |
|    | 495 nm                         | 3.4 s     | 480                 | 0.58                 |
|   | 510 nm                         | 1.6 min   | 245                 | 9.8                  |
|  | 520 nm                         | 20 min    | 41                  | 20                   |
|  | 550 nm                         | 10.5 min  | 16                  | 4.8                  |
|  | 540 nm                         | 15.6 s    | 206                 | 1.9                  |
|  | 590 nm                         | 2 min     | 39                  | 1.1                  |



Table 2 (Contd.)

| Phenoxy-1,2-dioxetane   | $\lambda_{\text{max}}$ CL [nm] | $t_{1/2}$ | Relative brightness | $\Phi_{\text{CL}}$ % |
|---|--------------------------------|-----------|---------------------|----------------------|
|    | 600 nm                         | 13.5 min  | 0.85                | 0.42                 |
|    | 600 nm                         | 3.3 s     | 65                  | 0.14                 |
|    | 610 nm                         | 11.9 min  | 0.25                | 0.073                |
|    | 610 nm                         | 31.2 s    | 8.3                 | 0.5                  |
|   | 660 nm                         | 5 min     | 0.24                | 0.13                 |
|  | 670 nm                         | 18 s      | 1.2                 | 0.012                |
|  | 710 nm                         | 17 min    | 0.61                | 0.38                 |

cells compared to LO2 cells indicated higher expression of FAP $\alpha$  in cancerous cells than in healthy ones (Fig. 5A). The selectivity of probes for endogenous enzymes was analysed by treating the cell lines with different concentrations of FAP $\alpha$  inhibitor (SP-13786). Furthermore, **CL-12a** was directly injected into the tumor and also injected into the tumor pre-treated with FAP $\alpha$  inhibitor (Fig. 5B). The higher chemiluminescence reported in the tumor site also proved the selectivity for endogenous FAP $\alpha$  and its applications for visualization of cancer cells.

**Granzyme B.** Granzyme B is a type of serine protease that is released into cancer cells by natural killer cells to trigger apoptotic cell death.<sup>71–73</sup> Through its proteolytic activity, granzyme B targets various intracellular proteins involved in apoptotic signalling pathways, ultimately dismantling the target cells. Recent studies provided insights into the multifaceted roles of granzyme B in immune regulation, inflammation, and tissue homeostasis.<sup>74</sup> To assay this enzyme, a probe (**CL-13**) was designed and synthesised by Vendrell and coworkers.<sup>71</sup> **CL-13** was meticulously crafted to target granzyme B with utmost pre-



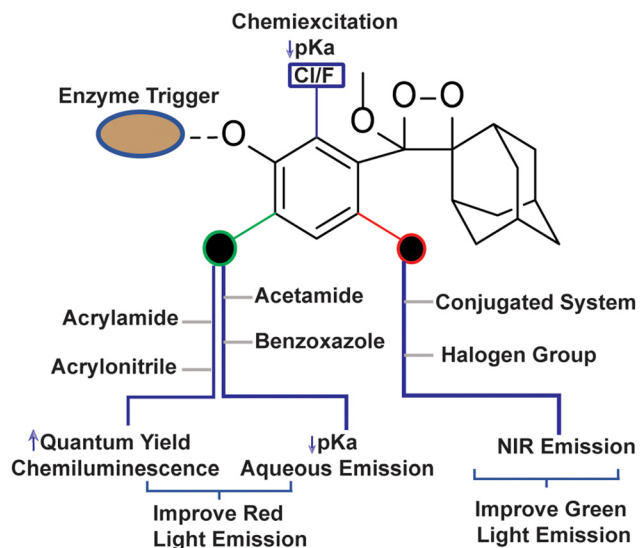


Fig. 4 Structure-activity relationship of phenoxy-1,2-dioxetane to tune physico-chemical Parameters.

cision and superior signal clarity amidst background noise. The probe comprises a phenolic hydroxyl group linked to an Ile-Glu-Pro-Asp peptide through a self-immolating linker. The authors found that within 10 minutes the incubation of CL-13 with granzyme B led to cleavage of the peptide linkage accompanied by 139-fold chemiluminescence enhancement at 520 nm. The varying concentrations of granzyme B showed linear enhancement in chemiluminescence with a detection limit of 0.7 nM. Furthermore, as shown in Fig. 5C, bright emis-

sion in MDA-MB cells co-cultured with NK cells as opposed to MDA-MB-231 signified higher expression of granzyme B in NK cells. Subsequently, CL-13 was administered into the tumor-contained NK cells, and live animal images were recorded immediately (Fig. 5D). Bright chemiluminescence signals were reported exclusively in the tumor area administered with NK cells *via* injection.

### 3.2 Aminopeptidases

**Aminopeptidase N (APN; EC 3.4.11.2).** Aminopeptidase N (APN) is an extracellular protease enzyme responsible for the cleavage of amino acid residues from the N-terminal of a substrate.<sup>75</sup> It is a widely distributed transmembrane ectoenzyme, participating in various physiological events, including cell migration, cell survival, angiogenesis, and viral uptake.<sup>76</sup> It is a well-known biomarker of hematopoietic cells, and its elevated expression facilitates tumor cell invasion.<sup>77</sup> The correlation between its expression levels and invasive capacity underscores APN's potential as a therapeutic target for cancer pathogenesis and its diagnosis.<sup>78</sup> Recently, numerous activatable chemiluminescence strategies have been adopted for monitoring APN activities. Lian and coworkers constructed an APN-triggered phenoxy-1,2-dioxetane derivative probe, CL-14.<sup>79</sup> The native chemiluminescence of the phenoxy-1,2-dioxetane nucleus was quenched by masking phenolic OH with an L-alanine motif through *para*-amino benzyl alcohol as a self-immolative linker. The probe was also decorated with an acrylonitrile group *ortho* to the phenol to improve quantum yield and luminosity time. Once hydrolysed by APN, the probe was rapidly activated and showed 26-fold chemiluminescence enhancement with a detection limit of 0.53 ng mL<sup>-1</sup>.

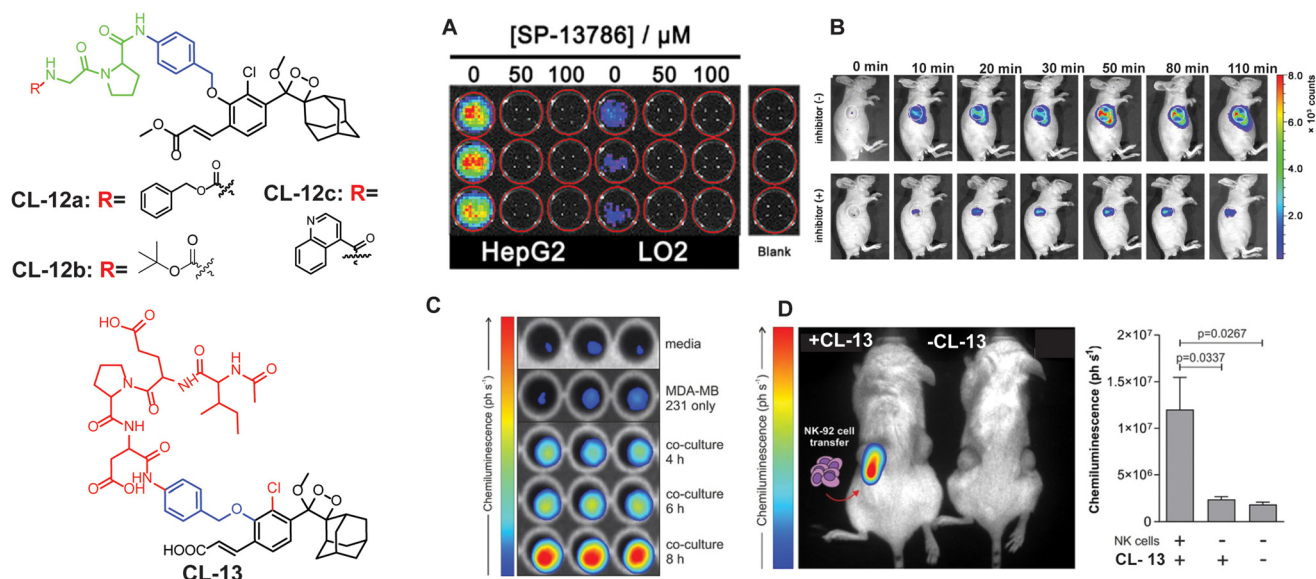


Fig. 5 Molecular structure of CL-12 and CL-13. (A) Chemiluminescence images of HepG2 and LO2 upon treatment with CL-12a. (B) Chemiluminescence response of CL-12 in animal models at different time intervals with and without inhibitor. (C) Chemiluminescence images of CL-13 incubated with media only, MDA-MB-231 cells alone, and co-cultures of MDA-MB-231 cells with NK-92 cells for the indicated times. (D) Chemiluminescence quantification in animal models. (A) and (B) are reproduced with permission.<sup>70</sup> Copyright © 2021 American Chemical Society. (C) and (D) reprinted with permission.<sup>71</sup> Copyright © 2021 Wiley-VCH.





Chemiluminescence signals linearly correlated to cell densities of HepG2 in the range of  $0.2 \times 10^4$  to  $2.0 \times 10^4$ . The primary approach to treat malignancies is through surgical procedures, which often provide the most effective chance for cure in many cases. The success of the surgery depends on the thoroughness of identifying and removing all aspects of the tumor, including its borders, microscopic elements, and any metastatic lesions. If the surgical resection is incomplete, there is a risk of the malignant tumors recurring. In this particular report, probe solution was sprayed around the tumor for *in situ* tumor imaging. The chemiluminescence emission intensity within the tumor tissue in animal models quickly increased, with a tumor-to-normal tissue ratio of  $1.2 \times 10^6$  being recorded (Fig. 6A) followed by image-guided surgical removal of tumor tissue that ensured the complete excision of cancerous cells (Fig. 6B). Instead of acrylonitrile, Gao and co-workers reported an acrylic ester-based chemiluminescent probe (CL-15) for image-guided tumor surgery.<sup>80</sup> It showed almost 190-fold chemiluminescence enhancement at 540 nm within 20 minutes of co-existence with APN. Moreover, its LOD ( $0.056 \text{ ng mL}^{-1}$ ) showed almost ten times higher sensitivity than that of CL-14. The chemiluminescence signal was detectable even at 20 mm thickness of chicken breast tissue with an extremely low background signal ( $174.2 \pm 30.2$ ). Therefore, CL-15 was employed to distinguish tumor tissues from normal tissues by directly spraying its aqueous solution on HepG2 xenograft tumors *ex vivo*, with normal liver tissue as control. It exhibited a high tumor-to-normal tissue ratio (T/N 160), which may be a promising approach for precise tumor resection. In an orthotopic HepG2-tumor mouse model, a luminescence signal reached a maximum value within 10 minutes post-injection

at the tumor site and, lasting for over 40 minutes (Fig. 6C and D), it may facilitate the removal of identified tumors under chemiluminescence guidance. Furthermore, Cao and coworkers replaced alanine with leucine to switch off the chemiexcitation and thus developed the CL-16 probe.<sup>81</sup> It showed 53-fold emission enhancement upon incubation with APN, and the detection limit was reported to be  $0.068 \text{ U mL}^{-1}$ . Cellular studies revealed that the probe is permeable through the cell membrane and its chemiluminescence was switched on in response to endogenous APN. The probe solution when injected into the tumor area showed a drastic increase in chemiluminescence intensity within 5 minutes of incubation and attained saturation in 20 minutes, while the tumor treated with an APN inhibitor did not show any noticeable emission. Based on the structure of these probes, we conclude that the presence of an acrylic ester group instead of an acrylonitrile group improved the detection limit with a better signal-to-noise ratio. This might be due to the more hydrophobic nature of the acrylic ester than the acrylic acid facilitating cell-membrane permeability.

**Leucine amino peptidase (LAP).** LAP (EC 3.4.11.1) is a proteolytic enzyme that belongs to M1 and M17 peptidases, which catalyse the cleavage of the peptide bond between the N-termini leucine residues in proteins.<sup>82</sup> Understanding the enzymatic activity of LAP is crucial for elucidating its role in physiological processes and exploring its potential as a target for therapeutic intervention in diseases where dysregulation of peptide metabolism is implicated. Cheng and coworkers explored chemiluminescence probes (CL-17a and CL-17b) that incorporated L-leucine into phenoxy-1,2-dioxetane to target LAP.<sup>83</sup> *In vivo* imaging is preferably achieved using NIR chemi-

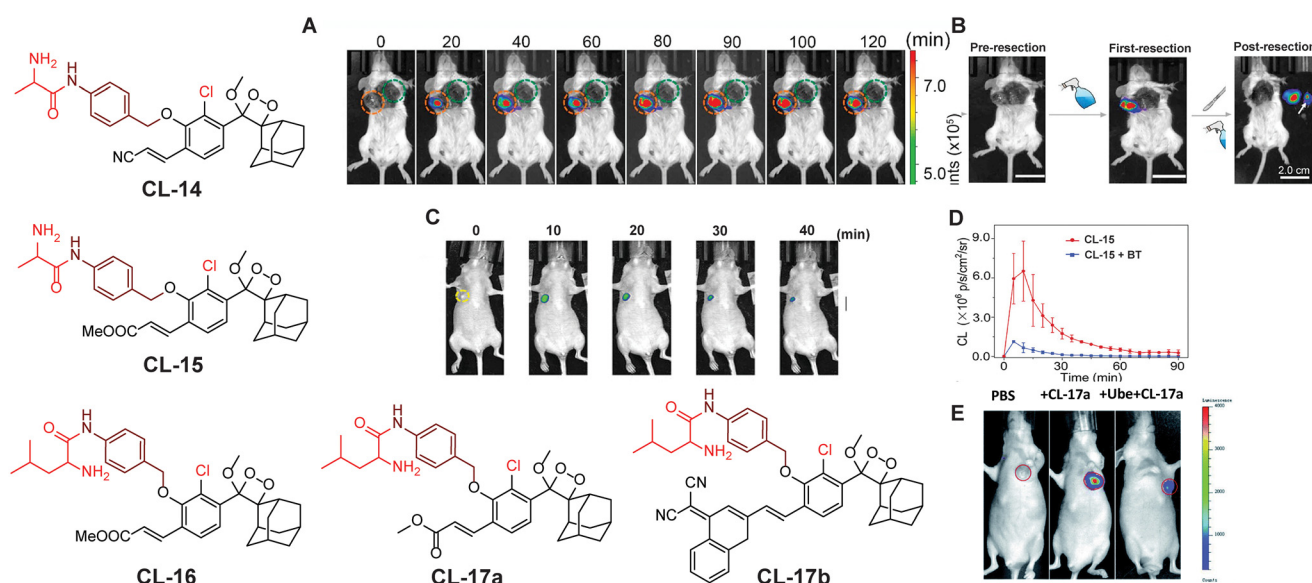


**Fig. 6** Chemiluminescence probes (CL-14 to CL-17b) for aminopeptidase N and leucine aminopeptidase. (A) Chemiluminescence images of 4T1-tumor-mice after spraying of CL-14. (B) Image-guided tumor surgery using CL-14. Reprinted with permission.<sup>79</sup> Copyright © 2022 Elsevier B.V. (C) Chemiluminescence images of a HepG2 xenograft after intra-tumoral injection of CL-15. (D) Quantification of the chemiluminescence signal of CL-15. (E) Live animal images of HepG2 tumor-containing mice. (C) and (D) reprinted with permission.<sup>80</sup> Copyright © 2022 Wiley-VCH GmbH. (E) is reproduced from ref. 83 with permission from the Royal Society of Chemistry. Copyright © 2022 Royal Society of Chemistry.

luminescence emission because of its superior depth penetration. **CL-17b** behaves as an NIR chemiluminescent probe because the  $\pi$ -electron system of the phenolic luminophore has been extended by inserting a dicyano methyl chromone group *ortho* to the phenol. The luminescence of **CL-17a** (a conventional probe) attained emission saturation at 550 nm within 20 minutes of LAP catalytic action. However, the NIR-emitting **CL-17b** remained inactive under similar conditions. Computational studies demonstrated that **CL-17b** faced steric hindrance when reaching the enzyme's active site due to its larger size, while **CL-17a** interacts through hydrogen bonding and thus is catalysed by LAP. It showed a signal-to-noise value of approximately 1260 with a detection limit of  $0.008 \text{ U mL}^{-1}$ . The greater chemiluminescence signal of HePG-2 cells compared to LO2 cells upon treatment with **CL-17a** justified the application for the differentiation of cancer cells from normal ones. Saturation of the chemiluminescence signal 10 minutes after injection into the tumor has also been reported by these authors. The selectivity of the probe was predicted by inhibiting LAP activity with Ube, followed by **CL-17a** treatment (Fig. 5E). Furthermore, cancerous liver tissue showed higher chemiluminescence intensity than normal tissues establishing the application potential of **CL-17a** for detection of LAP in clinical samples.

**Prostate-specific antigen (PSA, EC 3.4. 21.77).** Prostate-specific antigen is a serine protease enzyme that hydrolyses the amide linkage of peptide substrates after glutamine. It is a key biomarker in the realm of prostate cancer diagnosis, prognosis, and therapeutic monitoring.<sup>84,85</sup> Initially, it was identified for its role in liquefying seminal fluid but later garnered widespread attention due to its remarkable specificity to the prostate gland. Over the years, PSA has transitioned from a mere physiological marker to a crucial tool in the early detection of prostate cancer and semen analysis in criminal cases.<sup>86</sup> To target PSA, Portnoy and coworkers employed the Mu-HSSKLQ polypeptide, as a PSA trigger.<sup>87</sup> The chemiluminescence of *ortho* acrylic acid-substituted phenoxy-1,2-dioxetane is quenched with this peptide (**CL-18**). The cleavage of peptide bonds in the presence of PSA has led to a 157-fold change in emission intensity and 63-fold higher signal-to-noise ratio has been achieved as compared to a commercially available fluorescent probe. It distinctly underscores the superior PSA-detection capability of **CL-18** over fluorescent probes. Real-time semen samples showed 14-fold chemiluminescence compared to the control. Furthermore, the probe maintained its effectiveness even after three days (Fig. 7A and B) following sample preparation of human semen residues on fabric.

**Cathepsin B.** Cathepsin B is a lysosomal cysteine protease (EC 3.4.22.1) responsible for protein degradation, antigen processing, and tissue remodeling.<sup>88,89</sup> It is a dipeptidyl carboxypeptidase that removes two amino acid residues from the C-terminus of a peptide substrate. The occluding loop of the active pocket contains two histidine residues located at positions 110 and 111. These histidine residues act on the C-terminal carboxylate of the substrate, thereby aiding in the facilitation of the enzyme's exopeptidase activity.<sup>90</sup> Within lysosomes, cathepsins are involved in the digestion of proteins

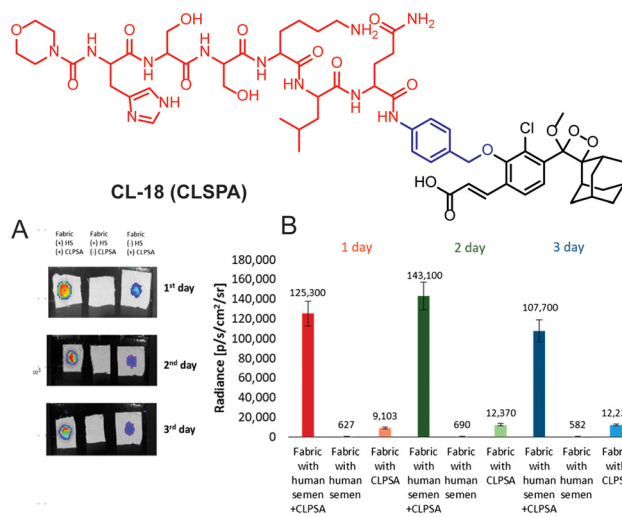


**Fig. 7** (A) Chemiluminescence images of human semen incubated with **CL-18** at different time intervals. (B) Chemiluminescence emission intensity quantification of (A). Reprinted with permission.<sup>87</sup> Copyright © 2020 American Chemical Society.

and peptides, breaking them down into amino acids that can be reused for building new proteins or generating energy. It is linked to various health issues such as neck, cervical, colon, breast, and ovarian cancers, as well as neurodegenerative diseases and inflammatory disorders. This makes it a promising target for therapeutics.<sup>91–93</sup> To trace its activity, Shabat and coworkers chose valine-Cit dipeptide as a substrate for cathepsin B.<sup>94</sup> **CL-19** is comprised of a conventional phenoxy-1,2-dioxetane scaffold bearing a cathepsin B-sensitive moiety, while **CL-20** is additionally decorated with an acrylic ester to enhance its chemiluminescence efficiency. The **CL-20** was further modified with 17-mer polyethylene glycol (PEG) and KRKGC peptide to improve its aqueous solubility and cell permeability (**CL-21** and **CL-22**). PEG is well known for its hydrophilic nature and has been extensively explored for drug delivery applications.<sup>95</sup> The peptide (KRKGC) comprises three positively charged residues, which enhance its solubility in an aqueous system and improve the cell membrane permeability.<sup>96</sup> With such modifications, **CL-21** showed better chemiluminescence response than **CL-19** and **CL-20**, while **CL-22** had even better chemiluminescence than **CL-21**. The superior chemiluminescence efficiency is attributed to the hydrophilic nature of these probes. Remarkably, **CL-22** showed a limit of detection  $76.29 \text{ U mL}^{-1}$ , which was 16 000-fold superior to its fluorescent analog. Due to the large expression of cathepsin B, RAW 264.7 and CT26 cells, except for 3T3 (the control group), showed bright chemiluminescence upon treatment with **CL-22**.<sup>97</sup> Furthermore, to achieve NIR emission, 12-(3,5,5-trimethylcyclohex-2-en-1-ylidene)malononitrile conjugated at the *para* position of phenoxy-1,2-dioxetane (**CL-23**) and the dipeptide “phenylalanine-lysine” were employed as a trigger for cathepsin B.<sup>63</sup> The conjugation of an extended  $\pi$  system at the *para* position increased the chemiluminescence quantum yield along with emission wavelength. The catalytic



action of cathepsin B led to 75.5-fold chemiluminescence enhancement at 650 nm within 30 minutes of incubation (Fig. 8A). For *in vivo* applications, the probe solution was injected intraperitoneally into 4T1-bearing tumor mouse models. The chemiluminescence emission attained maxima within 10 minutes of injection and it was 4-fold higher than the mouse pre-treated with cathepsin B inhibitor. Laparotomy was conducted 30 minutes after probe injection to illustrate the potential for precise tumor resection guided by chemiluminescence diagnosing deeply buried tumors (Fig. 8B). The fluorescence signal remained undetectable in the intestinal region compared to the chemiluminescence signal. The higher signal-to-background ratio (S/B 7.6) was reported for image-guided surgery in cathepsin B expressive tissues.

**Galactosidase.** Beta-galactosidase ( $\beta$ -Gal, EC.3.2.1.23) is a hydrolytic enzyme found in cell lysosomes that catalyses the breakdown of glycosidic linkages of oligosaccharides.<sup>98</sup> It is generally synthesised as an 88 kDa precursor protein followed by its transfer to the lysosome where it is further processed to a 64 kDa active protein.<sup>99,100</sup> The detection of  $\beta$ -Gal levels in the human body is critical in biomarking for diagnosing primary ovarian cancer and renal disease.<sup>101,102</sup> Elevated  $\beta$ -Gal activity can lead to the cleavage of the glycosidic bond within

the amino polysaccharide side chain and ultimately causes the breakdown of macromolecular proteoglycans and thus facilitates cancer metastasis.<sup>103</sup> Consequently, the development of  $\beta$ -Gal activatable probes holds significant importance, not only for assessing its activity but also for disease diagnosis. Numerous initiatives have been undertaken to monitor the increased activity of  $\beta$ -Gal in various preclinical cancer models. Due to the distinctive specificity for  $\beta$ -galactosyl bonds, it is possible to tailor the chemiluminescence of phenoxy-1,2-dioxetane for  $\beta$ -Gal detection. A common approach involves the functionalisation of phenolic OH with  $\beta$ -galactose as a protective group.  $\beta$ -Gal cleaves the  $\beta$ -galactose on addition of the substrate and thus triggers chemiluminescence.

This approach has been used by various research groups to develop numerous chemiluminescence probes. Initially, the chemiluminescence signals from Schaap's dioxetanes were enhanced through a process where energy from the excited state of the chemiluminophore was transferred to a nearby fluorophore.<sup>104,105</sup> This energy transfer led to increased light emission, serving as an indirect method to amplify chemiluminescence signals. Following a similar approach, Shabat and co-workers designed and synthesised Schaap's dioxetane-fluorophore conjugates (CL-24, CL-25, and CL-26) as NIR probes for

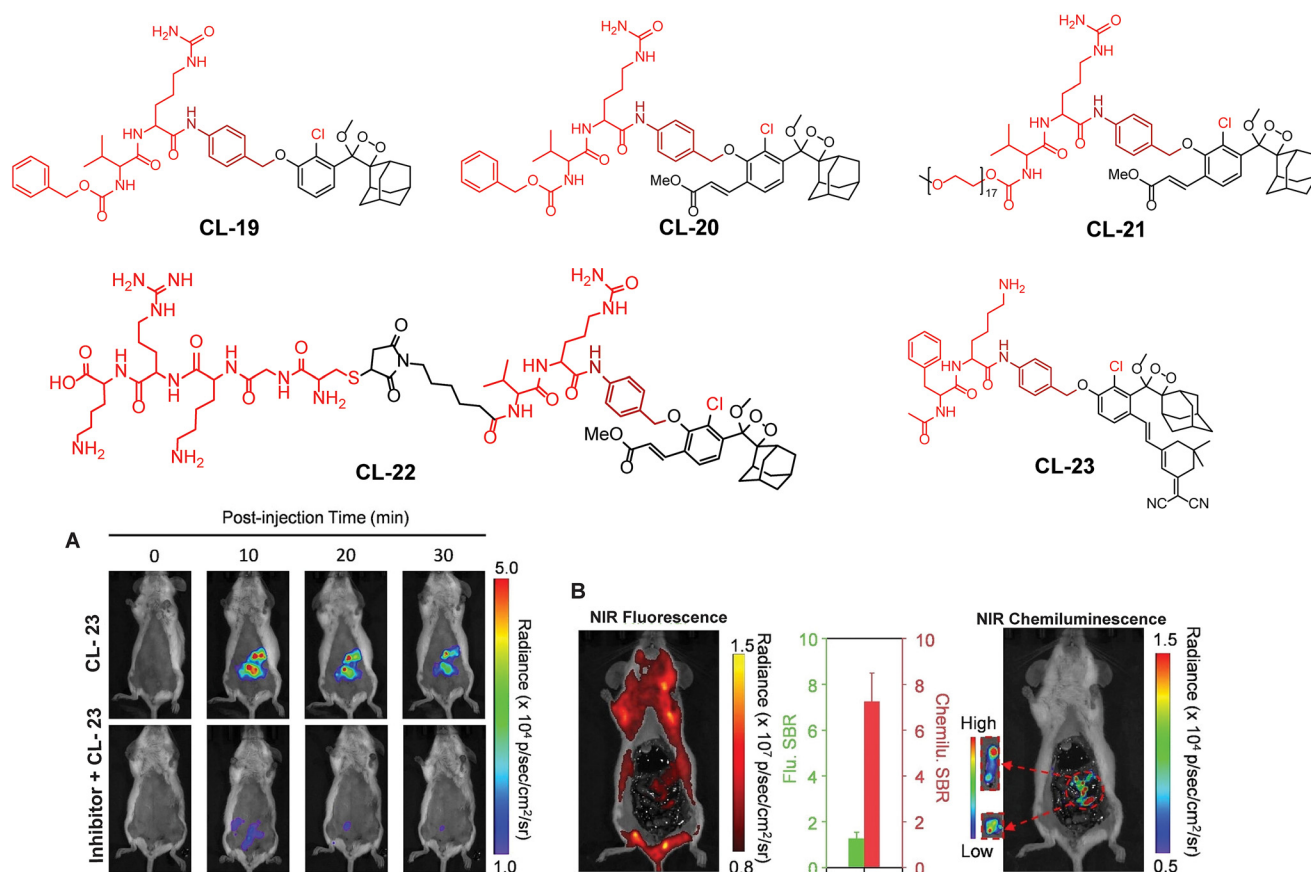


**Fig. 8** Chemical structure of probes CL-19 to CL-23. (A) Images of mice acquired at different time intervals after intraperitoneal injection of CL-23. (B) Fluorescence and chemiluminescence images of the intestine after laparotomy. (A) and (B) are reprinted with permission.<sup>63</sup> Copyright © 2022 Wiley-VCH GmbH.





detecting  $\beta$ -galactosidase ( $\beta$ -Gal) through covalent attachment of fluorophores.<sup>106</sup> Surprisingly, these probes suffered from light-induced photo-decomposition except for **CL-24**, which is a basic Schaap's-dioxetane derivative without tethering dye. **CL-25**, linked to fluorescein, was particularly unstable under light exposure ( $t_{1/2}$  = 45 minutes), compared to the more stable **CL-26** ( $t_{1/2}$  = 6 hours). Upon  $\beta$ -Gal activation, the emission spectrum of **CL-26** closely matched its fluorescence spectrum, confirming energy transfer from phenoxy-dioxetane to the fluorophore. **CL-26** produced a 25-fold chemiluminescence increase at 714 nm after  $\beta$ -Gal activation, while **CL-25** exhibited a 100-fold increase at 535 nm compared to **CL-24**. Furthermore, **CL-25** and **CL-26** were administered intraperitoneally into mice, with and without *ex vivo* exposure to  $\beta$ -Gal. Strikingly, **CL-26** generated a robust *in vivo* chemiluminescence image, whereas **CL-25** remained inactive without any chemiluminescence signal (Fig. 9). These results highlight the *in vivo* imaging superiority of the NIR-emitting **CL-26** compared to the short-wavelength emitting **CL-25** probe.

Probes using energy transfer mechanisms are structurally composed of two components: a 1,2-dioxetane moiety and a fluorescent dye. This combination increases the overall dimensions of the probe, which in turn limits its ability to access the active pockets of the enzyme. In contrast, a probe that consists of a smaller molecular structural framework enhances the binding interactions at the enzyme's catalytic site. Additionally, direct emitting probes exhibit superior photostability, and their chemical synthesis is comparatively

straightforward. By exploring the structure–activity relationship, Shabat and coworkers modified benzoate species with different electron-withdrawing groups (EWGs) to modulate the chemiluminescence efficiency and aqueous solubility of phenoxy-dioxetane probes.<sup>59</sup> They addressed the steric hindrance from *ortho* substituents by incorporating a self-immolative linker between the phenolic oxygen and the  $\beta$ -Gal substrate (probes **CL-27**, **CL-28**, **CL-29**, and **CL-30**). In the presence of  $\beta$ -Gal, **CL-27** showed a 500-fold stronger emission signal than **CL-24** in aqueous media. Interestingly, **CL-28** had similar emission amplification but with an improved kinetics profile, highlighting the role of the chlorine group in chemiexcitation. When the acrylic ester group was replaced with acrylonitrile (**CL-30**), 1800-fold higher chemiluminescence was observed compared to **CL-24**. The detection limits and kinetics parameters for these probes were not reported.

For further improvements in photophysical properties, the same group made significant advancements in developing NIR chemiluminescence turn-on probes by integrating an acceptor substituent with extended  $\pi$ -electron systems.<sup>61</sup> This integration allows increased emission efficiency, resulting in more sensitive and effective probes for biological imaging and detection applications. Probe **CL-31** was designed explicitly for  $\beta$ -Gal and exhibited a characteristic chemiluminescence kinetics profile with a 17-fold signal-to-noise ratio at 660 nm. The chemiluminescence intensity of transfected cells treated with **CL-31** was approximately 14 times higher than that of wild-type cells (Fig. 10A). Furthermore, Pu and coworkers developed

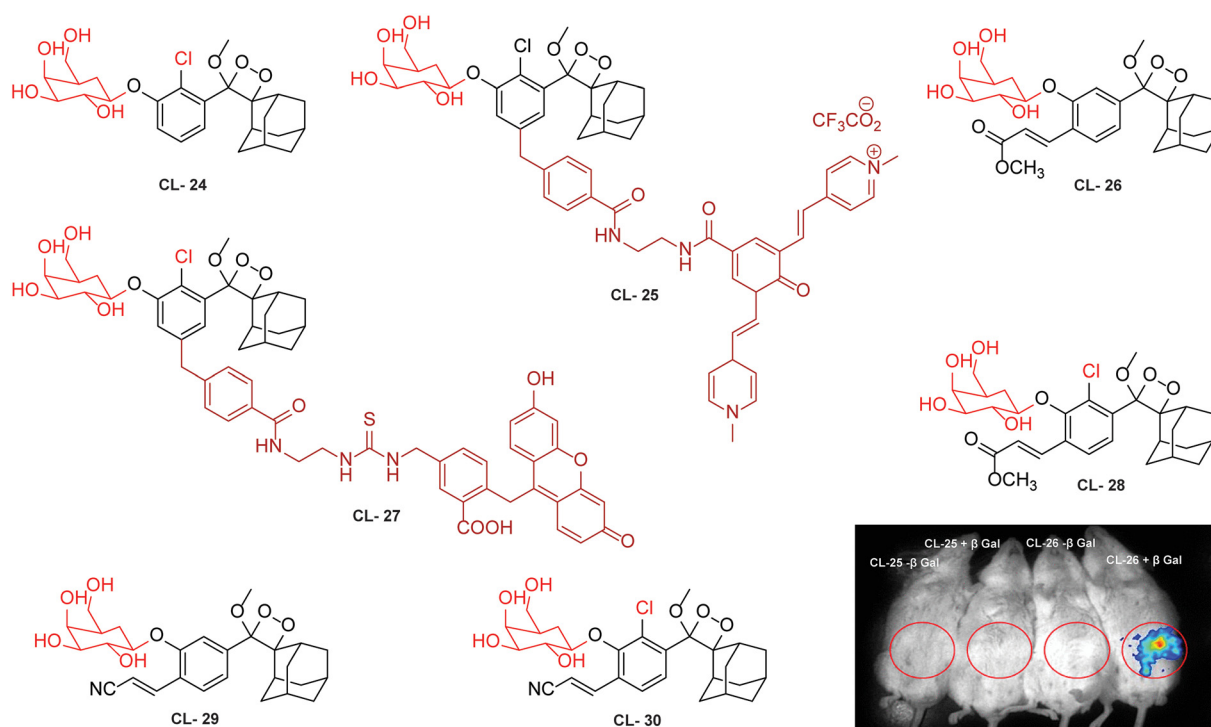
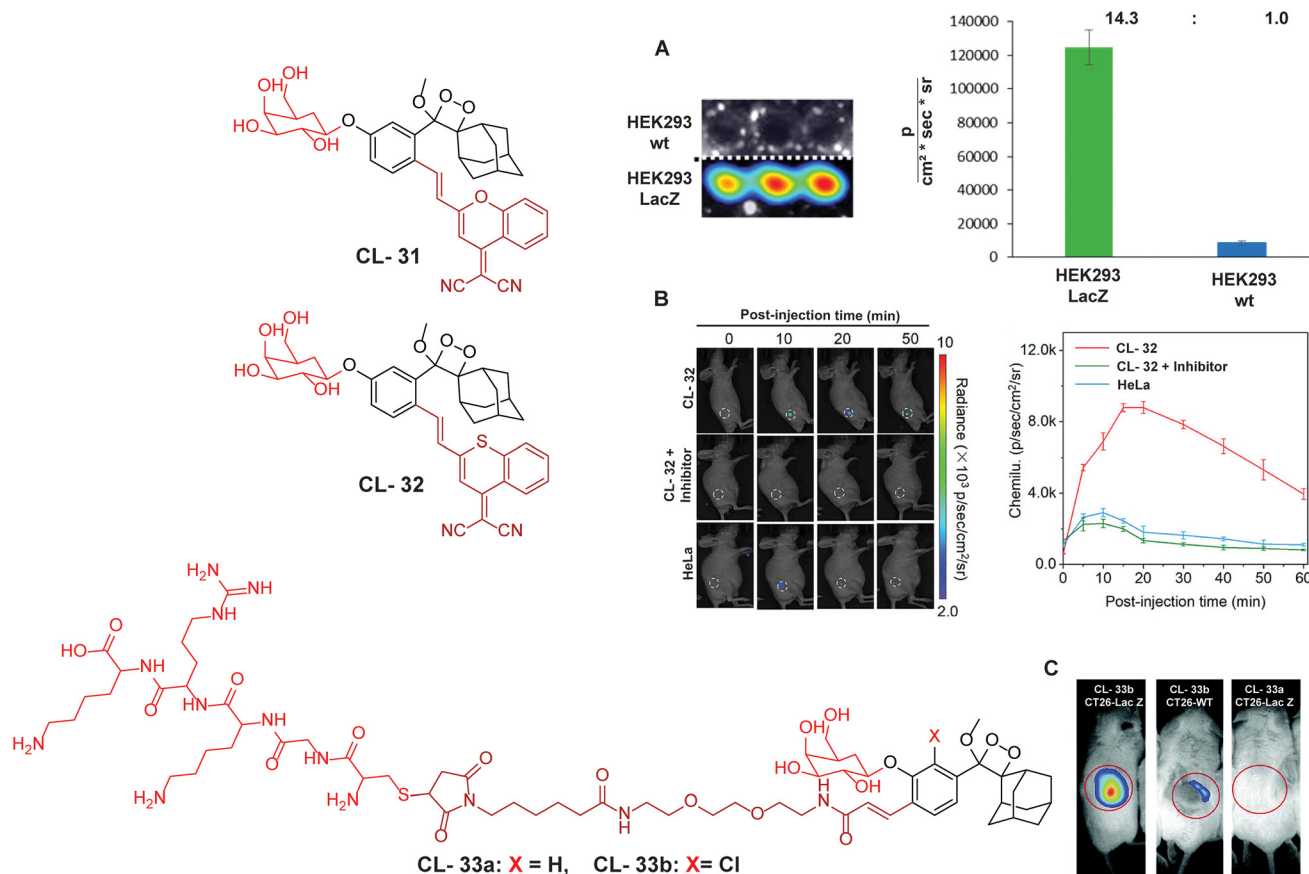


Fig. 9 Molecular structure of probes **CL-24** to **CL-30**. Whole body images after 15 minutes of intraperitoneal injection of **CL-25** and **CL-26**. (Probe solution incubated with  $\beta$ -Gal for 30 minutes prior to injection.) Reprinted with permission.<sup>106</sup> Copyright © 2016 American Chemical Society.





**Fig. 10** Molecular structure of probes CL-31 to CL-33. (A) Imaging of cell line upon treatment with CL-31 and quantification of emission intensity. Figure reproduced with permission.<sup>61</sup> Copyright © 2017, American Chemical Society (B) *In vivo* imaging of tumor-bearing mice upon treatment with CL-32. Reproduced with permission.<sup>62</sup> Copyright © 2020 Wiley-VCH GmbH. (C) *In vivo* imaging of tumor-bearing mice upon treatment with CL-33b. Reproduced with permission.<sup>109</sup> Copyright © 2018 Royal Society of Chemistry.

an NIR-emitting luminescent probe (CL-32) by conjugating dicyanomethylene-4*H*-benzothiopyran with a phenoxy-1,2-dioxetane moiety.<sup>62</sup> It showed 85.6-fold chemiluminescence enhancement when treated with  $\beta$ -Gal, with a detection limit of 73 mU L<sup>-1</sup>. SKOV3 cells exhibited a 13-fold increase in emission compared to HeLa cells within 30 minutes of treatment. In SKOV3 tumor-bearing mice, the chemiluminescence signal increased progressively after intratumoral injection, and at 20 minutes, SKOV3 tumors displayed a 6.5-fold higher signal compared to HeLa tumors (Fig. 10B). Despite these promising results, accurate delivery of such probes into cancer cells is a very challenging issue. Numerous strategies have been adopted to improve the cell specificity including anchoring a cell surface receptor-specific moiety to a cellular tracker.<sup>107,108</sup> In this regard, Shabat and coworkers anchored the tumor cell-specific peptide "CGKRR" to probe *via* a maleimide-based linker.<sup>109</sup> This approach not only improved the aqueous solubility but also directed the probe toward tumor cells.<sup>109</sup> The effectiveness of two probes, CL-33a and CL-33b, in imaging  $\beta$ -Gal activity was tested in mice with CT26 tumors. Direct injection of these probes into tumor sites showed that CT26-LacZ tumors injected with CL-33b exhibited a chemilumines-

cence signal approximately 20 times stronger than that of CT26-WT tumors, while CL-33a remained inactive (Fig. 10C). This significant enhancement in chemiluminescence was attributed to the lower p*K*<sub>a</sub> of the phenoxy-1,2-dioxetane bearing a chlorine substituent, which promoted chemiexcitation in the mildly acidic tumor microenvironment.

Monitoring low drug concentrations in individual patients is a challenge, impeding clinicians' ability to personalise treatments.<sup>110–112</sup> As a result, there is an apparent necessity for novel cancer therapies that not only minimise side effects but also enable real-time imaging of drug bio-distribution. One promising approach is to analyse drug release through chemiluminescence, which offers a superior signal-to-noise ratio in living tissues. Shabat and coworkers devised a theranostic prodrug, CL-34, to deliver monomethyl auristatin E in response to  $\beta$ -Gal activity.<sup>113</sup> The activation of this prodrug by  $\beta$ -Gal was accompanied by direct emission of green light, with a linear correlation between light emission at 555 nm and the release of the free drug. The activation of the prodrug with chemiluminescence enhancement is shown in Fig. 11A. In HEK293-LacZ cells, treatment with the prodrug led to a 25-fold increase in chemiluminescence compared to wild-type





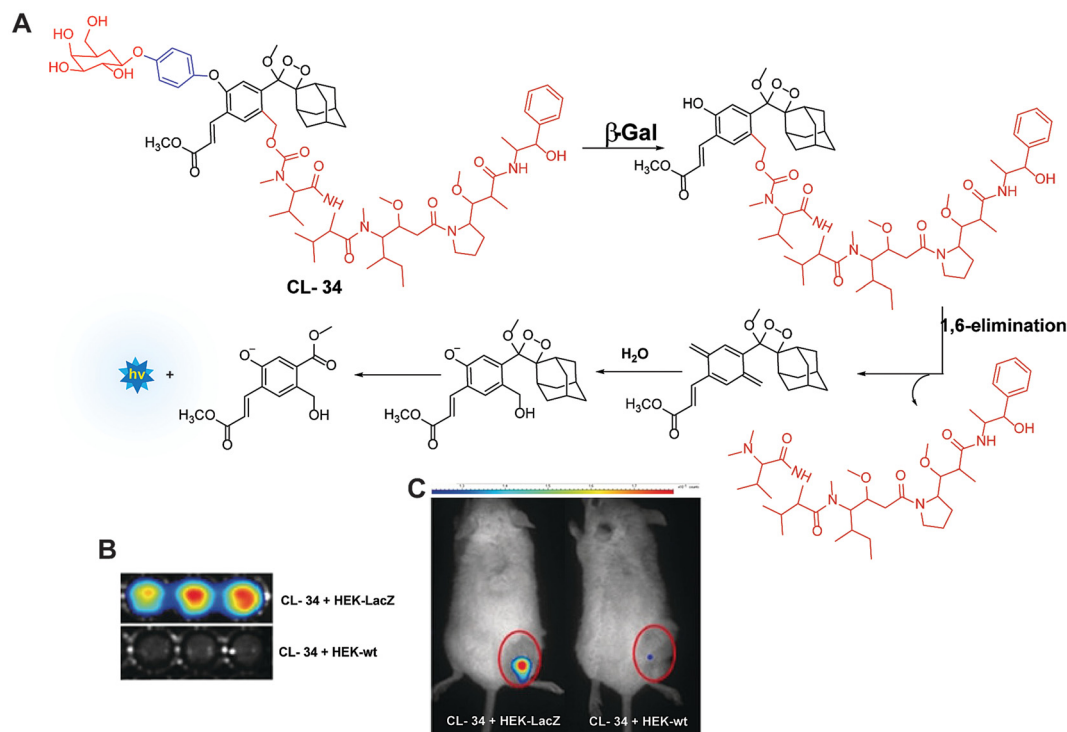


**Fig. 11** (A) Molecular mechanism of drug release from CL-34 in the presence of  $\beta$ -Gal. (B) Chemiluminescence images of mammalian cells upon treatment with prodrug. (C) Whole-body imaging of mice upon treatment with prodrug CL-34.<sup>113</sup> Copyright © 2018 Wiley-VCH Verlag GmbH & Co. KGaA, Weinheim.

HEK293 cells (Fig. 11B), and the  $IC_{50}$  was reduced by a factor of 20 in HEK293-LacZ cells. Increased chemiluminescence in HEK293-LacZ *versus* wild-type HEK293 revealed higher  $\beta$ -Gal expression. Additionally, mice bearing CT26-LacZ tumors treated with CL-34 showed approximately five times higher chemiluminescence compared to mice treated with the control prodrug (Fig. 11C).

**Esterases (EC 3.1).** Esterases are classified under the hydrolase class, capable of hydrolysis of esters into alcohols and acids. A wide range of enzymes, including acetylcholinesterase, carboxylesterase, lipase, *etc.* are classified under the hydrolase enzyme class.<sup>114,115</sup> They perform critical operations in biological systems such as ester metabolism, substance transportation, and gene expression. Their absence or abnormal expression leads to the pathogenesis of Wolman disease, cancer, and hyperlipidemia.<sup>116</sup> As a result, the development of novel and efficient esterase assays has considerable importance for the diagnosis and staging of numerous ailments. Recently, to monitor its activity, Chen and coworkers masked the phenolic OH of phenoxy-1,2-dioxetane with acetoxymethyl ether (CL-35). Hydrolysis of the ester bond in the presence of esterase was followed by release of phenoxy-1,2-dioxetane through a 1,6-elimination rearrangement reaction, as shown in Fig. 12A. The probe's emission reached saturation at 540 nm within 20 minutes, with a detection limit calculated to be  $1.90 \times 10^{-3} \text{ U mL}^{-1}$ .<sup>117</sup> Chemiluminescence intensity showed a linear relationship with varying esterase concentrations.

Additionally, a time-dependent change in emission was observed at the injection site when the probe solution, with or without esterase, was injected subcutaneously into animal models (Fig. 12B).

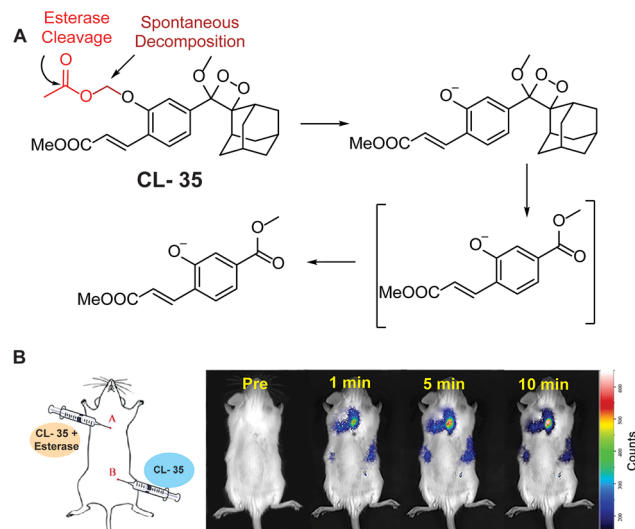


**Fig. 12** (A) Activation mechanism of CL-35 in the presence of esterase. (B) Chemiluminescence monitoring in animal models. Reprinted with permission.<sup>117</sup> Copyright © 2022 Elsevier B.V.



### 3.3 Oxidoreductase

**Nitroreductase (NTR).** NTR is a flavin-containing redox enzyme that participates in the reduction of nitro-containing compounds in organisms.<sup>118</sup> Under hypoxic conditions, it facilitates the electron transfer reduction of nitro groups to hydroxylamines, subsequently converting them into amines in the presence of nicotinamide adenine dinucleotide (NADH).<sup>119</sup> Based on their catalytic activity, NTRs are categorised into two types: type I, which are oxygen-insensitive, and type II, which are oxygen-sensitive.<sup>120</sup> Type II NTRs facilitate the one-electron transfer reduction of nitro groups, producing superoxide anions. Type I NTRs are further subdivided into major and minor groups based on their cofactor preferences. This class of enzymes functions as homodimers with flavin mononucleotide (FMN)-binding sites necessary for their activity. They operate through a ping-pong bi-bi redox mechanism, utilising a nicotinamide cofactor to transfer electrons and reduce nitroaromatic compounds.<sup>121,122</sup> Due to their close association with hypoxic environments in living cells, NTRs have been extensively studied for imaging of cancer cells and drug delivery applications. In tumor microenvironments, hypoxia often leads to increased levels of NTR; however, it is scarcely expressed in normal tissues.<sup>123,124</sup> Numerous NTR-responsive chemiluminescent probes and drug delivery systems have been developed, and extensively utilised for cellular imaging.<sup>125,126</sup>

Lippert and coworkers utilised the *para*-nitrobenzyl moiety as a triggering substrate (CL-36 and CL-37) for the imaging of NTR.<sup>42</sup> The *para*-nitrobenzyl group underwent self-immolative cleavage when exposed to an enzyme in the presence of NADH. This process led to liberation of phenolate-1,2-dioxetane,

which subsequently underwent the CIEEL mechanism and emits light. Furthermore, the chemiluminescence intensity increased with the addition of 10% Emerald II. Emerald II is an aqueous solution that contains a polymer that imparts a hydrophobic environment for the chemiluminophore and thus diminishes the quenching effect of water molecules. Probe CL-37 showed significantly improved signal-to-noise ratio (172-fold) and selectivity over biothiols compared to CL-36. The limit of detection calculated for CL-37 was 1.9 ng mL<sup>-1</sup>. In experiments with tumor xenograft SCID/BALB-C mice, hypoxic conditions were maintained in environments with 21% and 100% oxygen. Notably, the animals exposed to oxygen-deficient conditions exhibited brighter chemiluminescence than those in oxygen-rich environments (Fig. 13A). However, the authors found that use of cationic polymers caused toxicity to living tissues and thus limited their clinical applicability.<sup>127</sup> To address this issue, Zhang and coworkers synthesised a water-soluble probe (CL-38) by introducing an electron-withdrawing carboxylate substituent *ortho* to the NTR trigger.<sup>128</sup> This probe showed 6000-fold chemiluminescence enhancement upon incubation with NTR/NADH even without an additional enhancer and had a detection limit of 0.947 ng mL<sup>-1</sup>, significantly surpassing that of CL-36. Furthermore, the probe solution was injected intratumorally to visualise the degree of hypoxia in A459 tumor-bearing mouse models. The chemiluminescence of CL-38 correlated directly with the tumor's hypoxic state (Fig. 13B), revealing a mean photon flux intensity in hypoxic mice 4.5 times greater than in mice with sufficient oxygen. While probes CL-37 and CL-38 responded to tissue oxygenation in animal models, studies of their use on cell lines were not explored. To fill this gap, Lippert and co-

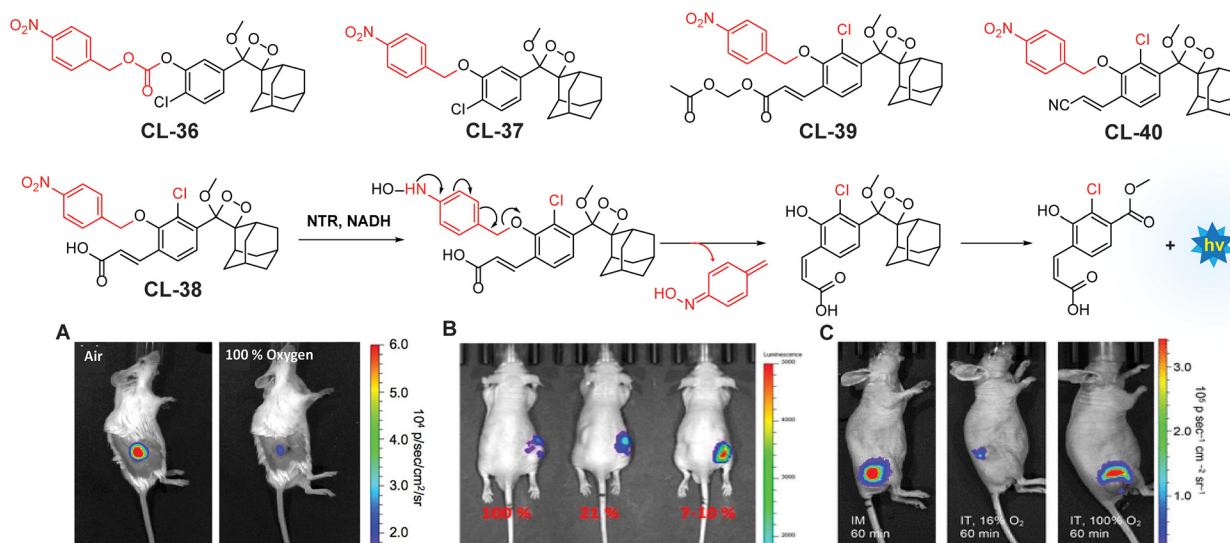


**Fig. 13** Molecular structure of probes CL-36 to CL-40. (A) Images of living H1299 lung-tumor-bearing mice 1.5 min after administering intratumoral injections of CL-37 and 10% Emerald II enhancer. Figure reproduced with permission.<sup>42</sup> Copyright © 2016 American Chemical Society. (B) Images of tumor (A459) within 10 minutes of intratumoral injection of CL-38. Reproduced with permission.<sup>128</sup> Copyright © 2018 American Chemical Society. (C) Images of animal models bearing tumor after injection with CL-40. Figure reproduced with permission.<sup>129</sup> Copyright © 2019 American Chemical Society.



workers reported the effectiveness of **CL-39** and **CL-40** chemiluminescent reporters for hypoxia across various settings: *in vitro*, within cellular environments, and *in vivo*.<sup>129</sup> **CL-40** showed 37-fold chemiluminescence enhancement in 80 minutes in rat liver microsomes, while **CL-39** exhibited an

extraordinary 60 000-fold enhancement in just 20 minutes. The drastic increase in chemiluminescence response and ultra-sensitivity of **CL-39** was attributed to acetoxymethyl ester, which improved its cellular uptake. Additionally, **CL-40** was successfully utilised to discriminate between hypoxic and nor-

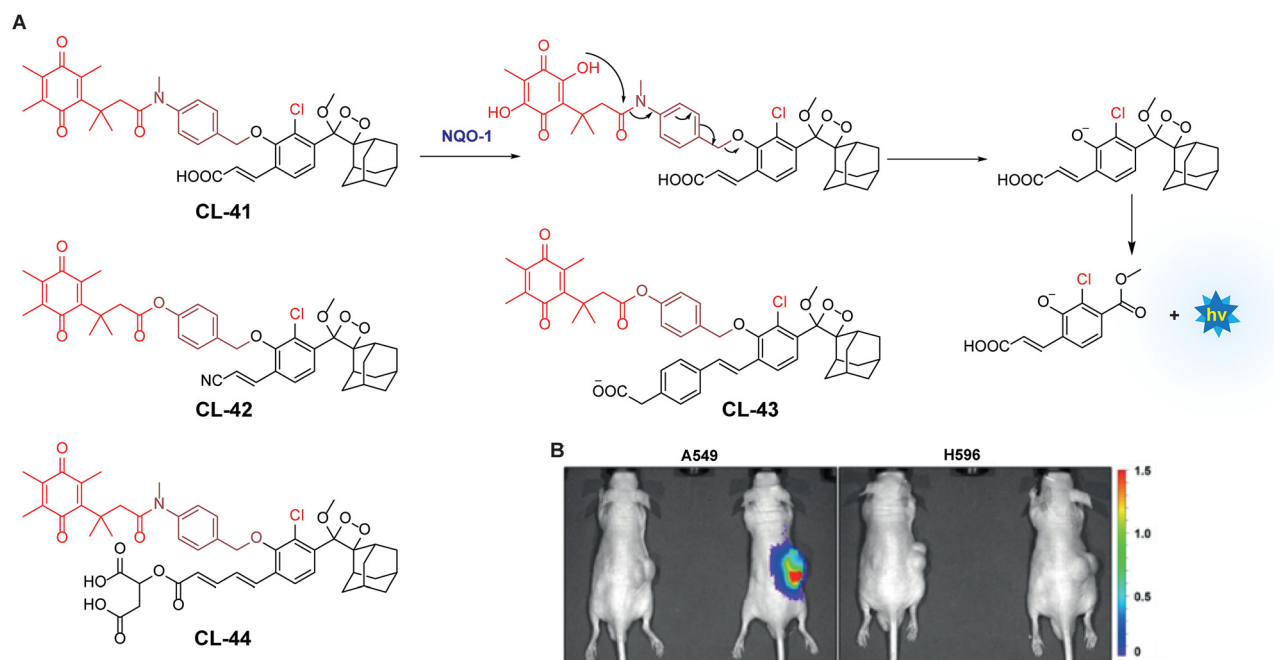


**Fig. 14** (A) Activation mechanism of **CL-41** in the presence of NQO1. (B) *In vivo* imaging of NQO1 upon treatment with **CL-41**. Reprinted with permission.<sup>133</sup> Copyright © 2019 Wiley-VCH Verlag GmbH & Co. KGaA, Weinheim.

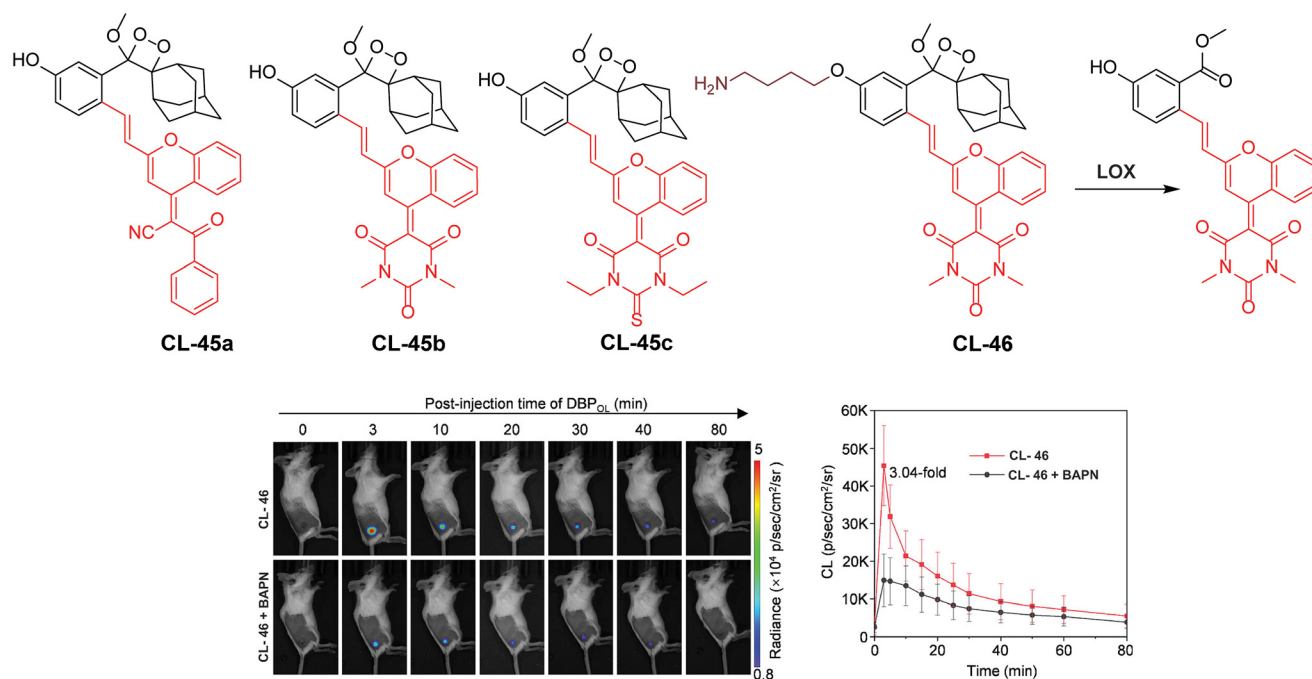


**Fig. 15** Molecular structure of probes **CL-45** and **CL-46**. Chemiluminescence images of animal models upon treatment with **CL-46** and quantification of emission intensity.<sup>138</sup> Copyright © 2023 Wiley-VCH GmbH.





moxic conditions in A549 cells, with images taken 60 minutes post-injection revealing distinct contrasts between hypoxic and well-oxygenated tissues (Fig. 13C). The photon flux intensity ( $1 \times 10^7$  photons per s) of CL-39 was 100 times greater than that of CL-37 and CL-NTR. These findings suggest that positioning of EWG substituents at the *para* position of phenolic OH is a critical component of the process to improve chemiluminescence emission and sensitivity. Moreover, integrating hydrophobic groups, such as esters, alongside EWGs could further facilitate cellular uptake. Future structural modifications may enhance the photophysical properties and cellular uptake of phenoxy-1,2-dioxetane derivatives.

**NAD(P)H quinone oxidoreductase 1 (DT-diaphorase; EC 1.6.5.2).** NAD(P)H quinone oxidoreductase 1 is an intracellular flavoenzyme that regulates the redox state by facilitating the two-electron reduction reaction of quinones toward their respective hydroquinones.<sup>130</sup> It works almost with similar efficiency in the presence of cofactors NADPH or NADH. It is a homodimer having two active pockets where the FAD cofactor is bound tightly.<sup>131</sup> Its significant overexpression (5–200-fold) in numerous types of tumors makes it responsible for multiple carcinogenic processes. This heightened expression in tumors highlights the necessity for developing sensitive probes that can detect cancer subtypes associated with high NQO1 levels.<sup>132</sup> To track NQO1 activity in both *in vitro* and *in vivo* models, chemiluminophores are generally conjugated with quinone-based substrates that undergo bio-reduction. Kim and coworkers investigated chemiluminescence of phenoxy-1,2-dioxetane by covalently tethering it with trimethyl-locked quinone through a self-immolative linker (CL-41).<sup>133</sup> This probe, when bio-catalysed by NQO1, showed 130-fold chemiluminescence enhancement at 515 nm, with a detection limit of  $51 \text{ ng mL}^{-1}$ . The quinone reduction mechanism followed by light emission is shown in Fig. 14A. Additionally, A549 cells showed 34 times more chemiluminescence than H596 cells when treated with CL-41. NQO1 activity was also visualised in A549 and H596-derived xenografts, where A549 tumor-bearing mice showed strongly bright chemiluminescence while no apparent signal was obtained in H596 ones (Fig. 14B). Shabat

and coworkers extended this work by synthesising acrylonitrile (CL-42) and styryl-substituted probes (CL-43) to detect varying concentrations of NADH in the presence of NQO1. CL-42 showed more rapid chemiexcitation than CL-41, with a limit of detection of 8 nM, while CL-43 exhibited 4-fold higher sensitivity, achieving a detection limit of 2 nM. This improvement is attributed to the styryl group, which enhances the reactivity of phenolate anions. Later, the same group designed the probe CL-44 to improve the emission wavelength and aqueous solubility.<sup>43</sup> It showed remarkable 310-fold emission enhancement at 610 nm in response to NQO1. However, mammalian cell line studies were not conducted with this probe.

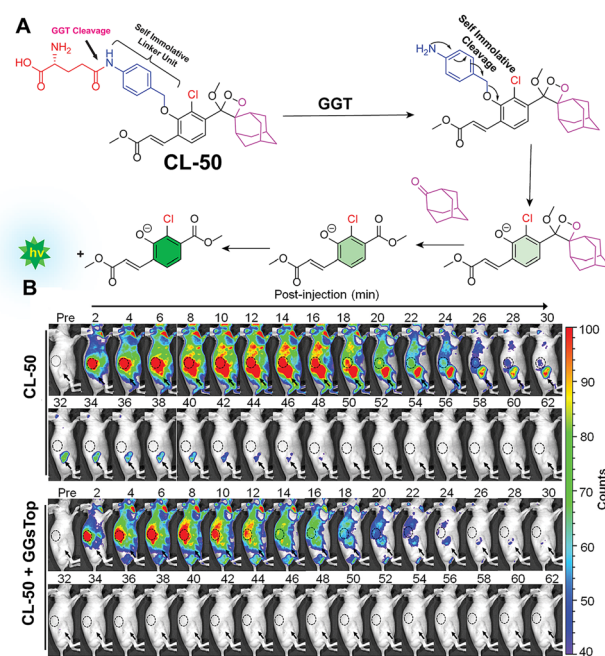


**Fig. 17** (A) Activation mechanism of CL-50 upon incubation with glutamyl transpeptidase. (B) Real-time chemiluminescence images of U87MG-tumor-bearing mice after injection of CL-50. Reprinted with permission.<sup>145</sup> Copyright © 2019 American Chemical Society.

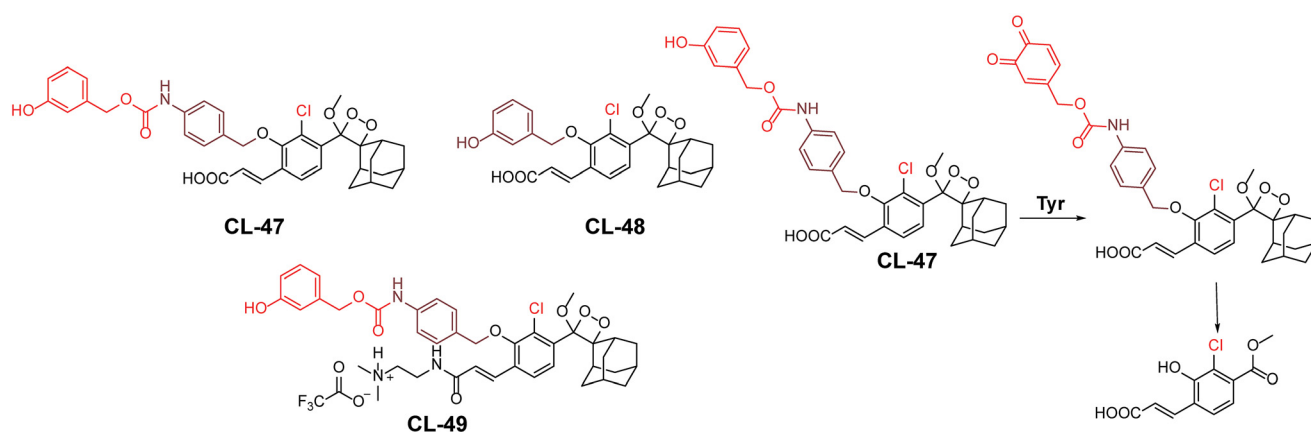


**Fig. 16** Molecular structure of probes CL-47 to CL-49 and the reaction mechanism outline for tyrosinase detection.



**Lysyl oxidase (LOX).** Lysyl oxidase is a protein-lysine 6-oxidase (EC 1.4.3.13), which catalyses the deamination reaction of amino acids to promote cross-linking in collagen and elastin tissues, thereby enhancing the structural integrity of

the ECM proteins.<sup>134,135</sup> The enzyme's catalytic site contains copper-binding domains, which are essential for its activity. LOX is an ECM protein secreted by tumor cells to foster tumor growth and metastasis.<sup>136,137</sup> Consequently, LOX has garnered

**Table 3** Summary of phenoxy-1,2-dioxetane derivatives discussed in this review

| Probe  | Enzyme              | LOD                                      | Mice/injection                              | Fold enhancement | $\lambda_{em}$ (nm) | Cell type                | $\Phi_{CL}$ (Einstein per mol) | $T_{1/2}$   | Ref. |
|--------|---------------------|--|---|------------------|---------------------|--------------------------|--------------------------------|-------------|------|
| CL-12a | FAP $\alpha$        | 0.785 ng mL <sup>-1</sup>                | 6-Week-old male BALB/c nude mice, IT        | 121              | —                   | HepG2                    | —                              | —           | 70   |
| CL-12c | FAP $\alpha$        | 0.965 ng mL <sup>-1</sup>                | —   | —                | —                   | HepG2                    | —                              | —           |      |
| CL-12c | FAP $\alpha$        | 0.587 ng mL <sup>-1</sup>                | —   | —                | —                   | HepG2                    | —                              | —           |      |
| CL-13  | Granzyme B          | 0.7 nM                                   | NSG mice, IT                                | 139              | 520                 | NK cells                 | —                              | —           | 71   |
| CL-14  | Aminopeptidase N    | 0.53 ng mL <sup>-1</sup>                 | Nude BABL/c mice                            | 26               | 510                 | HepG2                    | —                              | —           | 79   |
| CL-15  | Aminopeptidase N    | 0.056 ng mL <sup>-1</sup>                | 3–5-Week-old BALB/c nude mice               | —                | 540                 | HepG2                    | —                              | —           | 80   |
| CL-16  | Aminopeptidase N    | 0.068 U mL <sup>-1</sup>                 | 6-Week-old BALB/c nude mice, IT             | 53               | 560                 | HepG2 and LO2            | —                              | —           | 81   |
| CL-17a | LAP                 | 0.008 U mL <sup>-1</sup>                 | 4–5-Week-old BALB/c nude mice, IT           | 1260             | 550                 | HepG2 and LO2            | —                              | —           | 83   |
| CL-17b | LAP                 | Inactive                                 | —   | —                | —                   | —                        | —                              | —           |      |
| CL-18  | PSA                 | —  | —   | 157              | —                   | —                        | —                              | —           | 87   |
| CL-22  | Cathepsin B         | 76.29 mU mL <sup>-1</sup>                | —   | —                | 540                 | RAW 246.7, CT26, and 3T3 | —                              | —           | 97   |
| CL-23  | Cathepsin B         | —  | —   | 75.5             | 650                 | 4T1                      | —                              | —           | 63   |
| CL-24  | $\beta$ -Gal        | —  | —   | —                | —                   | —                        | —                              | —           |      |
| CL-25  | $\beta$ -Gal        | $4.0 \times 10^{-3}$ units per mL        | BALB/c female mice, IP                      | 100              | 535                 | HEK293-LacZ              | $3.8 \times 10^{-3}$           | 170 min     | 106  |
| CL-26  | $\beta$ -Gal        | —  | BALB/c female mice, IP                      | 25               | 714                 | HEK293-LacZ              | $9.0 \times 10^{-4}$           | 100 minutes |      |
| CL-31  | $\beta$ -Gal        | —  | —   | 17               | 660                 | HEK293-LacZ              | $0.82 \times 10^{-2}$          | 178 minutes | 61   |
| CL-32  | $\beta$ -Gal        | 73 mU mL <sup>-1</sup>                   | Adult female Ncr nude mice, IT              | 85.6             | 760                 | SKOV3                    | $0.23 \times 10^{-2}$          | 62 seconds  | 62   |
| CL-33a | $\beta$ -Gal        | —  | 7-Week-old BALB/c female mice, IT           | —                | —                   | CT26                     | —                              | —           | 109  |
| CL-33b | $\beta$ -Gal        | —  | 7-Week old BALB/c female mice, IT           | 30               | —                   | CT26                     | —                              | —           |      |
| CL-34  | $\beta$ -Gal        | —  | BALB/c, IT                                  | 25               | 555                 | HEK293-LacZ              | —                              | —           | 113  |
| CL-35  | Esterase            | $1.90 \times 10^{-3}$ U mL <sup>-1</sup> | —   | —                | 540                 | HeLa                     | —                              | —           | 117  |
| CL-37  | NTR                 | 1.9 ng mL <sup>-1</sup>                  | 6-Week old BALB/c female mice, IT           | 172              | 545                 | —                        | —                              | —           | 42   |
| CL-38  | NTR                 | 0.947 ng mL <sup>-1</sup>                | SCID/BALB-C, IT                             | 6000             | —                   | —                        | —                              | —           | 128  |
| CL-39  | NTR                 | —  | —   | 60 000           | 516                 | —                        | —                              | —           | 129  |
| CL-40  | NTR                 | —  | Athymic nude mice                           | 37               | 525                 | A549                     | —                              | —           |      |
| CL-41  | NQO1                | 51 ng mL <sup>-1</sup>                   | —   | 130              | 515                 | A549                     | —                              | —           | 132  |
| CL-42  | NQO1                | 8 nM for NADH                            | —   | —                | —                   | —                        | —                              | —           | 60   |
| CL-43  | NQO1                | 2 nM for NADH                            | —   | —                | —                   | —                        | —                              | —           |      |
| CL-44  | NQO1                | —  | —   | 310              | 610                 | —                        | —                              | —           | 43   |
| CL-46  | LOX                 | 0.013 U mL <sup>-1</sup>                 | BALB/c mice (female, 5 weeks old), IT       | 19.1             | 720                 | 4T1                      | —                              | —           | 138  |
| CL-47  | Tyrosinase          | 0.1 U mL <sup>-1</sup>                   | —   | 430              | 540                 | B16                      | —                              | —           | 141  |
| CL-50  | $\gamma$ -Glutamate | 16 mL U <sup>-1</sup>                    | Female, athymic, 6–8 weeks old, BALB/c mice | 876              | —                   | U87MG                    | —                              | —           | 145  |





significant attention as a potential therapeutic target in cancer treatment, and efforts are underway to develop a synthetic chemiluminescent reporter for monitoring LOX activity. Pu and coworkers developed activatable chemiluminescent probes for targeted photodynamic cancer therapy (PDT).<sup>138</sup> They modified the malononitrile group of dicyanomethylene-4*H*-benzopyran-phenoxy-dioxetane by replacing it with benzoylacetone, 1,3-dimethylbarbituric acid, and 1,3-diethyl-2-thio-barbituric acid to narrow the energy gap. Three different probes (**CL-45a**, **CL-45b**, and **CL-45c**) have been developed and further modified to track LOX activity. These probes exhibited chemiluminescence emissions redshifted to 700, 738, and 742 nm with half-lives of 178, 62, and 114 minutes, respectively. Based on the highest single oxygen-generating capacity of **CL-45b** for PDT, its chemiluminescence was masked with propylamine to target LOX (**CL-46**). Upon activation by LOX within 30 minutes, **CL-46** showed a remarkable 19.1-fold enhancement in chemiluminescence, with a limit of detection of 0.013 U mL<sup>-1</sup>. Mice bearing 4T1 tumors were injected with a probe intratumorally followed by immediate chemiluminescence imaging for 80 minutes, achieving peak brightness in just 3 minutes (Fig. 15). The tumor-to-background ratio was reported to be 14.6, which was 3.04 times higher than that observed in the  $\beta$ -aminopropionitrile (LOX inhibitor) group. Subsequently, light irradiation for PDT resulted in complete inhibition of tumor growth.

**Tyrosinase.** Tyrosinase is a copper-containing metalloenzyme (EC 1.14.18.1) involved in the synthesis of melanin pigment in the skin.<sup>139</sup> It catalyses the *ortho*-hydroxylation of monophenol to diphenol, followed by formation of the corresponding quinone, and leads to an unusual accumulation of melanin in skin cells.<sup>140</sup> Due to its ability to oxidise small phenolic molecules, the chemiluminophores are modified with triggering units containing *para*- or *meta*-phenol groups. Based on the enzyme-substrate reaction mechanism, Sessler and coworkers developed tyrosine-based chemiluminescent probes (**CL-47**, **CL-48**, and **CL-49**).<sup>141</sup> In this system, tyrosinase-mediated catalysis leads to the formation of stable *ortho*-benzoquinone intermediates, resulting in a poor chemiluminescence response. However, when thiols are introduced, they fully reduce the intermediate through 1,6-elimination, releasing benzoate intermediates, resulting in robust chemiluminescence (Fig. 16). The addition of thiols to the reaction solution improved the chemiexcitation by 430-fold compared to the response with tyrosinase alone. Thiol conjugation to benzoquinone promoted the 1,6-elimination reaction and resulted in enhanced chemiexcitation. For **CL-47**, the detection limit was determined to be 0.1 U mL<sup>-1</sup> with varying enzyme concentrations in the presence of glutathione. The inferior response of **CL-48** compared to **CL-47** is attributed to its sterically hindered structure. Additionally, the presence of a carboxylic group limited cell permeability, leading to further modification of **CL-47** by adding a 2-dimethylaminoethyl group to create **CL-49**. Notably, **CL-49** exhibited a 2.6-fold higher chemiluminescent response in B16 cells compared to EMT6 cells, indicating its ability to differentiate between cell lines.

However, the inherent limitation of the 'AND' logic operation lies in the inability to monitor tyrosinase activity independently without adding thiols. This highlights significant demands for a system capable of monitoring two species through independent emission channels.

### 3.4 Transferase

Gamma-glutamyl transpeptidase (EC 2.3.2.2) is a cell membrane-bound transferase enzyme crucial for maintaining glutathione and cysteine homeostasis by breaking down  $\gamma$ -glutamate in glutathione.<sup>142,143</sup> Abnormal activity of this enzyme is associated with liver dysfunction, asthma, diabetes, and the pathogenesis of cancer.<sup>144</sup> Therefore, researchers have been tracing its activity noninvasively in living cells and animal models to identify the diseased cells. Ye and coworkers employed modified Schaap's dioxetane substituted with an acrylic ester to track the activity of glutamyl transpeptidase (**CL-50**).<sup>145</sup> Similar to previous probes, this probe incorporates a phenoxy-1,2-dioxetane structure anchored with the recognition unit of  $\gamma$ -glutamic acid, facilitating interaction with the enzyme's active site (Fig. 17A). It showed a significant 876-fold increase in chemiluminescence within 30 minutes of incubation with glutamyl transpeptidase. The chemiluminescence peaked in intensity within 15 minutes and remained detectable for over 45 minutes in OVCAR5 and U87MG cells. In these cancer cells, the average chemiluminescence intensity was approximately 29-fold and 23-fold higher, respectively, compared to HUVEC cells. In tumor-bearing mice, intravenous administration showed a gradual increase in chemiluminescence up until 12 minutes before returning close to background levels after 1 hour (Fig. 17B). Inhibition of glutamyl transpeptidase activity with GGsTop in U87MG tumors suppressed the chemiluminescence during imaging. Quantitative analysis revealed that the intensity of chemiluminescence in cancerous cells treated with **CL-50** was 2.1 times greater than in tumors treated with GGsTop. A summary of the phenoxy-1,2-dioxetane derivatives is provided in Table 3.

## 4 Conclusion and perspective

This review highlights the advancements in phenoxy-1,2-dioxetanes as chemiluminophores for diagnostic applications, focusing on a multidisciplinary approach that combines expertise in organic chemistry, biochemistry, cell biology, and photophysics. Tables 1 and 2 present various design strategies for chemiluminophores aimed at enhancing the photophysical properties of phenoxy-1,2-dioxetanes, such as emission maxima, quantum yields, and p*K*<sub>a</sub> values. Meanwhile, Table 3 provides an overview of different 1,2-dioxetane chemiluminophores, categorised based on their selectivity for specific enzyme classes relevant to various diseases and their use in bio-imaging applications.

Despite the advances in activatable probes for bio-imaging, research on chemiluminescence-based approaches remains in its early stages. The reported chemiluminescent probes for



imaging endogenous enzymes meet several obstacles including low emission intensity, emission at shorter wavelengths, and shorter luminescence lifetimes. Therefore, extensive investigation into structural modifications of phenoxy-1,2-dioxetanes is needed to enhance chemiexcitation, emission wavelength, and luminescence half-life. Previously, various methods have been employed to achieve near-infrared (NIR) emission for deep-tissue imaging, including the conjugation of fluorescent dyes with phenoxy-1,2-dioxetane and the addition of electron-withdrawing groups (EWGs) at the *ortho* and *para* positions of the phenol group. However, these approaches increase the overall size of the probe, limiting its ability to enter the enzyme's active site and often resulting in compromised quantum yields. Therefore, more structural modifications are necessary to improve the brightness. Additionally, tuning the  $pK_a$  of the phenolic OH group is critically important for effective bio-imaging at physiological pH. The kinetics parameters, including the Michaelis–Menten constant and  $V_{max}$ , are crucial in determining the affinity of these probes for particular enzymes. However, this study was not conducted for the chemiluminescent probes discussed in this review. Evaluating parameters such as  $K_{cat}$  and the substrate's association constant with the enzyme could significantly enhance the design strategies for enzyme-specific probes.

Among the wide range of enzymes involved in cellular metabolism and disease progression, only a few have garnered attention for the development of chemiluminescent probes. The continuous advancements in chemical biology and medicinal chemistry are expected to enhance our understanding of the precise reaction sites within enzymes and biomarkers, paving the way for the development of new chemiluminescent enzyme probes. We anticipate that these probes will emerge as indispensable tools in both diagnostics and theranostics. This review provides valuable insights for aspiring researchers entering this field.

## Data availability

No primary research results, software, or code have been included and no new data were generated or analysed as part of this review.

## Conflicts of interest

All the authors declare no conflict of interest.

## Acknowledgements

J. S. Sidhu acknowledges the BITS-Pilani, Pilani campus for providing infrastructure and research facilities. MKC would like to thank the Royal Society of Chemistry (R23-0850952021) and University of Kent for funding.

## References

- 1 M. Zhao, B. Li, H. Zhang and F. Zhang, *Chem. Sci.*, 2021, **12**, 3448–3459.
- 2 V. Naresh and N. Lee, *Sensors*, 2021, **21**, 1109.
- 3 S. He, J. Song, J. Qu and Z. Cheng, *Chem. Soc. Rev.*, 2018, **47**, 4258–4278.
- 4 E. A. Owens, M. Henary, G. El Fakhri and H. S. Choi, *Acc. Chem. Res.*, 2016, **49**, 1731–1740.
- 5 J. A. Thomas, *Chem. Soc. Rev.*, 2015, **44**, 4494–4500.
- 6 A. Fernández and M. Vendrell, *Chem. Soc. Rev.*, 2016, **45**, 1182–1196.
- 7 S. Yoon, S. Y. Cheon, S. Park, D. Lee, Y. Lee, S. Han, M. Kim and H. Koo, *Biomater. Res.*, 2022, **26**, 57.
- 8 A. Ji, H. Lou, J. Li, Y. Hao, X. Wei, Y. Wu, W. Zhao, H. Chen and Z. Cheng, *Chem. Sci.*, 2024, **15**, 3339–3348.
- 9 Y. Shi, Y. Hu, N. Jiang and A. K. Yetisen, *ACS Sens.*, 2022, **7**, 1615–1633.
- 10 W. L. Rice, D. M. Shcherbakova, V. V. Verkhusha and A. T. N. Kumar, *Cancer Res.*, 2015, **75**, 1236–1243.
- 11 O. Green, T. Eilon, N. Hananya, S. Gutkin, C. R. Bauer and D. Shabat, *ACS Cent. Sci.*, 2017, **3**, 349–358.
- 12 Y. Yang, S. Wang, L. Lu, Q. Zhang, P. Yu, Y. Fan and F. Zhang, *Angew. Chem., Int. Ed.*, 2020, **59**, 18380–18385.
- 13 Y. Liu, J. Tan, M. Wan, L. Zhang and X. Yao, *ACS Omega*, 2020, **5**, 15922–15930.
- 14 A. Lyu, Y. Wang and H. Cui, *Anal. Chem.*, 2023, **95**, 7914–7923.
- 15 A. Roda, M. Mirasoli, E. Michelini, M. Di Fusco, M. Zangheri, L. Cevenini, B. Roda and P. Simoni, *Biosens. Bioelectron.*, 2016, **76**, 164–179.
- 16 S. Emdadi, M. H. Sorouraddin and L. Denanny, *Analyst*, 2021, **146**, 1326–1333.
- 17 X. Lu, X. Song, Q. Wang, W. Hu, W. Shi, Y. Tang, Z. Wu, Q. Fan and W. Huang, *RSC Adv.*, 2020, **10**, 11861–11864.
- 18 U. Haris and A. R. Lippert, *ACS Sens.*, 2023, **8**, 3–11.
- 19 H. Gunduz, T. Almammadov, M. Dirak, A. Acari, B. Bozkurt and S. Kolemen, *RSC Chem. Biol.*, 2023, **4**, 675–684.
- 20 Y. Yang and F. Zhang, *Analysis Sensing*, 2021, **1**, 75–89.
- 21 A. V. Romanyuk, I. D. Grozdova, A. A. Ezhov and N. S. Melik-Nubarov, *Sci. Rep.*, 2017, **7**, 3410.
- 22 M. A. Tzani, D. K. Gioftsidou, M. G. Kallitsakis, N. V. Pliatsios, N. P. Kalogiouri, P. A. Angaridis, I. N. Lykakis and M. A. Terzidis, *Molecules*, 2021, **26**, 7664.
- 23 L. Yue and Y.-T. Liu, *J. Phys. Chem. B*, 2020, **124**, 7682–7693.
- 24 H. An, C. Guo, D. Li, R. Liu, X. Xu, J. Guo, J. Ding, J. Li, W. Chen and J. Zhang, *ACS Appl. Mater. Interfaces*, 2020, **12**, 17230–17243.
- 25 R. C. Allen, *Antioxidants*, 2022, **11**, 518.
- 26 H. Karatani, *Anal. Sci.*, 2022, **38**, 613–621.
- 27 J. Zhang, C. Wickizer, W. Ding, R. Van, L. Yang, B. Zhu, J. Yang, Y. Wang, Y. Wang, Y. Xu, C. Zhang, S. Shen, C. Wang, Y. Shao and C. Ran, *Proc. Natl. Acad. Sci. U. S. A.*, 2023, **120**, e2310131120.



- 28 D. Calabria, M. Guardigli, M. Mirasoli, A. Punzo, E. Porru, M. Zangheri, P. Simoni, E. Pagnotta, L. Ugolini, L. Lazzeri, C. Caliceti and A. Roda, *Anal. Biochem.*, 2020, **600**, 113760.
- 29 C. Bourlieu, T. Astruc, S. Barbe, J.-G. Berrin, E. Bonnin, R. Boutrou, V. Hugouvieux, S. Le Feunteun and G. Paës, *Biotechnol. Adv.*, 2020, **41**, 107546.
- 30 J. S. Sidhu, N. Kaur and N. Singh, *Biosens. Bioelectron.*, 2021, **191**, 113441.
- 31 M. R. Bond and J. A. Hanover, *Annu. Rev. Nutr.*, 2013, **33**, 205–229.
- 32 R. Gupta, R. K. Ambasta and P. Kumar, *Life Sci.*, 2020, **243**, 117278.
- 33 J. Zhang, X. Chai, X.-P. He, H.-J. Kim, J. Yoon and H. Tian, *Chem. Soc. Rev.*, 2019, **48**, 683–722.
- 34 M. David, Q. Jaber, M. Fridman and D. Shabat, *Chem. – Eur. J.*, 2023, **29**, e202300422.
- 35 H. N. Kagalwala, R. T. Reeves and A. R. Lippert, *Curr. Opin. Chem. Biol.*, 2022, **68**, 102134.
- 36 A. P. Schaap, R. S. Handley and B. P. Giri, *Tetrahedron Lett.*, 1987, **28**, 935–938.
- 37 A. P. Schaap, T.-S. Chen, R. S. Handley, R. DeSilva and B. P. Giri, *Tetrahedron Lett.*, 1987, **28**, 1155–1158.
- 38 A. P. Schaap, M. D. Sandison and R. S. Handley, *Tetrahedron Lett.*, 1987, **28**, 1159–1162.
- 39 S. Gutkin, S. Gandhesiri, A. Brik and D. Shabat, *Bioconjugate Chem.*, 2021, **32**, 2141–2147.
- 40 L. Liu and R. P. Mason, *PLoS One*, 2010, **5**, e12024.
- 41 J. Cao, R. Lopez, J. M. Thacker, J. Y. Moon, C. Jiang, S. N. S. Morris, J. H. Bauer, P. Tao, R. P. Mason and A. R. Lippert, *Chem. Sci.*, 2015, **6**, 1979–1985.
- 42 J. Cao, J. Campbell, L. Liu, R. P. Mason and A. R. Lippert, *Anal. Chem.*, 2016, **88**, 4995–5002.
- 43 S. Gutkin, R. Tannous, Q. Jaber, M. Fridman and D. Shabat, *Chem. Sci.*, 2023, **14**, 6953–6962.
- 44 S. Gutkin, R. Tannous, Q. Jaber, M. Fridman and D. Shabat, *Chem. Sci.*, 2023, **14**, 6953–6962.
- 45 A. Fu, Y. Mao, H. Wang and Z. Cao, *J. Pharm. Biomed. Anal.*, 2021, **204**, 114266.
- 46 J. C. Hummelen, T. M. Luider and H. Wynberg, in *Methods Enzymol.*, Academic Press, 1986, vol. 133, pp. 531–557.
- 47 L. F. M. L. Ciscato, F. H. Bartoloni, A. S. Colavite, D. Weiss, R. Beckert and S. Schramm, *Photochem. Photobiol. Sci.*, 2014, **13**, 32–37.
- 48 M. Yang, J. Zhang, D. Shabat, J. Fan and X. Peng, *ACS Sens.*, 2020, **5**, 3158–3164.
- 49 K. J. Bruemmer, O. Green, T. A. Su, D. Shabat and C. J. Chang, *Angew. Chem.*, 2018, **130**, 7630–7634.
- 50 M. Vacher, I. F. Galván, B.-W. Ding, S. Schramm, R. Berraud-Pache, P. Naumov, N. Ferré, Y.-J. Liu, I. Navizet, D. Roca-Sanjuán, W. J. Baader and R. Lindh, *Chem. Rev.*, 2018, **118**, 6927–6974.
- 51 W. Adam, I. Bronstein, A. V. Trofimov and R. F. Vasil'ev, *J. Am. Chem. Soc.*, 1999, **121**, 958–961.
- 52 L. F. M. L. Ciscato, F. H. Bartoloni, D. Weiss, R. Beckert and W. J. Baader, *J. Org. Chem.*, 2010, **75**, 6574–6580.
- 53 H. Takakura, *Molecules*, 2021, **26**, 1618.
- 54 P. Farahani, M. A. Oliveira, I. F. Galván and W. J. Baader, *RSC Adv.*, 2017, **7**, 17462–17472.
- 55 C. Dodeigne, L. Thunus and R. Lejeune, *Talanta*, 2000, **51**, 415–439.
- 56 I. Bronstein, B. Edwards and J. C. Voyta, *J. Biolumin. Chemilumin.*, 1989, **4**, 99–111.
- 57 Y. Hisamatsu, T. Fukiage, K. Honma, A. G. Balia, N. Umezawa, N. Kato and T. Higuchi, *Org. Lett.*, 2019, **21**, 1258–1262.
- 58 J. Huang, P. Cheng, C. Xu, S. S. Liew, S. He, Y. Zhang and K. Pu, *Angew. Chem., Int. Ed.*, 2022, **61**, e202203235.
- 59 O. Green, T. Eilon, N. Hananya, S. Gutkin, C. R. Bauer and D. Shabat, *ACS Cent. Sci.*, 2017, **3**, 349–358.
- 60 N. Hananya, J. P. Reid, O. Green, M. S. Sigman and D. Shabat, *Chem. Sci.*, 2019, **10**, 1380–1385.
- 61 O. Green, S. Gnaim, R. Blau, A. Eldar-Boock, R. Satchi-Fainaro and D. Shabat, *J. Am. Chem. Soc.*, 2017, **139**, 13243–13248.
- 62 J. Huang, Y. Jiang, J. Li, J. Huang and K. Pu, *Angew. Chem., Int. Ed.*, 2021, **60**, 3999–4003.
- 63 X. Wei, J. Huang, C. Zhang, C. Xu, K. Pu and Y. Zhang, *Angew. Chem., Int. Ed.*, 2023, **62**, e202213791.
- 64 G. Blum, G. von Degenfeld, M. J. Merchant, H. M. Blau and M. Bogoy, *Nat. Chem. Biol.*, 2007, **3**, 668–677.
- 65 E. A. Mason, R. Lopez and R. P. Mason, *Opt. Mater. Express*, 2016, **6**, 1384–1392.
- 66 A. A. Fitzgerald and L. M. Weiner, *Cancer Metastasis Rev.*, 2020, **39**, 783–803.
- 67 Z. Yu, Y. Huang, H. Chen, Z. Jiang, C. Li, Y. Xie, Z. Li, X. Cheng, Y. Liu, S. Li, Y. Liang and Z. Wu, *ACS Pharmacol. Transl. Sci.*, 2023, **6**, 1745–1757.
- 68 L. Zhang, W. Ying, Z. Sheng, L. Lv, J. Gao, Y. Xue and L. Liu, *Anal. Biochem.*, 2022, **655**, 114859.
- 69 K. Dienus, A. Bayat, B. F. Gilmore and O. Seifert, *Arch. Dermatol. Res.*, 2010, **302**, 725–731.
- 70 A. Fu, H. Wang, T. Huo, X. Li, W. Fu, R. Huang and Z. Cao, *Anal. Chem.*, 2021, **93**, 6501–6507.
- 71 J. I. Scott, S. Gutkin, O. Green, E. J. Thompson, T. Kitamura, D. Shabat and M. Vendrell, *Angew. Chem., Int. Ed.*, 2021, **60**, 5699–5703.
- 72 I. Voskoboinik, J. C. Whisstock and J. A. Trapani, *Nat. Rev. Immunol.*, 2015, **15**, 388–400.
- 73 J. A. Trapani, *Genome Biol.*, 2001, **2**, DOI: [10.1186/gb-2001-2-12-reviews3014](https://doi.org/10.1186/gb-2001-2-12-reviews3014).
- 74 J. E. Davis, V. R. Sutton, M. J. Smyth and J. A. Trapani, *Cell Death Differ.*, 2000, **7**, 973–983.
- 75 S. A. Amin, N. Adhikari and T. Jha, *J. Med. Chem.*, 2018, **61**, 6468–6490.
- 76 A. J. Turner, Membrane alanyl aminopeptidase, in *Handbook of Proteolytic Enzymes*, 2004, pp. 289–294. DOI: [10.1016/B978-0-12-079611-3.50077-X](https://doi.org/10.1016/B978-0-12-079611-3.50077-X). Epub 2012 Dec 2.
- 77 M. Alfalah, M. P. Krahn, G. Wetzels, S. von Hörsten, C. Wolke, N. Hooper, T. Kalinski, S. Krueger, H. Y. Naim and U. Lendeckel, *J. Biol. Chem.*, 2006, **281**, 11894–11900.



- 78 S.-X. Cui, X.-J. Qu, Z.-H. Gao, Y.-S. Zhang, X.-F. Zhang, C.-R. Zhao, W.-F. Xu, Q.-B. Li and J.-X. Han, *Cancer Lett.*, 2010, **292**, 153–162.
- 79 X. Shi, Y. Deng, X. Liu, G. Gao, R. Wang and G. Liang, *Biosens. Bioelectron.*, 2022, **208**, 114212.
- 80 Y. Liu, J. Zeng, Q. Li, M. Miao, Z. Song, M. Zhao, Q. Miao and M. Gao, *Adv. Opt. Mater.*, 2022, **10**, 2102709.
- 81 R. Sun, X. Wu, Y. Mao, H. Wang, C. Bian, P. Lv, Z. Zhao, X. Li, W. Fu, J. Lu and Z. Cao, *Luminescence*, 2022, **37**, 1335–1342.
- 82 M. B. Harbut, G. Velmourougane, S. Dalal, G. Reiss, J. C. Whisstock, O. Onder, D. Brisson, S. McGowan, M. Klemba and D. C. Greenbaum, *Proc. Natl. Acad. Sci. U. S. A.*, 2011, **108**, E526–E534.
- 83 B. Wang, Z. Chen, X. Cen, Y. Liang, L. Tan, E. Liang, L. Zheng, Y. Zheng, Z. Zhan and K. Cheng, *Chem. Sci.*, 2022, **13**, 2324–2330.
- 84 M. J. Ahrens, P. A. Bertin, E. F. Vonesh, T. J. Meade, W. J. Catalona and D. Georganopoulou, *Prostate*, 2013, **73**, 1731–1737.
- 85 A. P. Drabovich, P. Saraon, K. Jarvi and E. P. Diamandis, *Nat. Rev. Urol.*, 2014, **11**, 278–288.
- 86 P. Suttipasit and S. Wongwittayapanich, *J. Forensic Leg. Med.*, 2018, **54**, 102–108.
- 87 S. Gutkin, O. Green, G. Raviv, D. Shabat and O. Portnoy, *Bioconjugate Chem.*, 2020, **31**, 2488–2493.
- 88 V. Turk, V. Stoka, O. Vasiljeva, M. Renko, T. Sun, B. Turk and D. Turk, *Biochim. Biophys. Acta, Proteins Proteomics*, 2012, **1824**, 68–88.
- 89 M. C. Yoon, V. Hook and A. J. O'Donoghue, *Biochemistry*, 2022, **61**, 1904–1914.
- 90 T. R. Lambeth, Z. Dai, Y. Zhang and R. R. Julian, *RSC Chem. Biol.*, 2021, **2**, 606–611.
- 91 A. Amritraj, K. Peake, A. Kodam, C. Salio, A. Merighi, J. E. Vance and S. Kar, *Am. J. Pathol.*, 2009, **175**, 2540–2556.
- 92 H. Dong, Y. Qin, Y. Huang, D. Ji and F. Wu, *Neurochem. Int.*, 2019, **126**, 178–186.
- 93 K. Ditaranto, T. L. Tekirian and A. J. Yang, *Neurobiol. Dis.*, 2001, **8**, 19–31.
- 94 M. E. Roth-Konforti, C. R. Bauer and D. Shabat, *Angew. Chem., Int. Ed.*, 2017, **56**, 15633–15638.
- 95 J. M. Harris and R. B. Chess, *Nat. Rev. Drug Discovery*, 2003, **2**, 214–221.
- 96 J. A. Hoffman, E. Giraudo, M. Singh, L. Zhang, M. Inoue, K. Porkka, D. Hanahan and E. Ruoslahti, *Cancer Cell*, 2003, **4**, 383–391.
- 97 M. E. Roth-Konforti, C. R. Bauer and D. Shabat, *Angew. Chem., Int. Ed.*, 2017, **56**, 15633–15638.
- 98 S. Chen, X. Ma, L. Wang, Y. Wu, Y. Wang, W. Fan and S. Hou, *Sens. Actuators, B*, 2023, **379**, 133272.
- 99 A. T. Hoogveen, F. W. Verheijen and H. Galjaard, *J. Biol. Chem.*, 1983, **258**, 12143–12146.
- 100 S. Zhang, J. McCarter, Y. Okamura-Oho, F. Yaghi, A. Hinek, S. Withers and J. Callahan, *Biochem. J.*, 1994, **304**, 281–288.
- 101 M. Li, M. Yang and W.-H. Zhu, *Mater. Chem. Front.*, 2021, **5**, 763–774.
- 102 D. Asanuma, M. Sakabe, M. Kamiya, K. Yamamoto, J. Hiratake, M. Ogawa, N. Kosaka, P. L. Choyke, T. Nagano, H. Kobayashi and Y. Urano, *Nat. Commun.*, 2015, **6**, 6463.
- 103 J. Zhang, P. Cheng and K. Pu, *Bioconjugate Chem.*, 2019, **30**, 2089–2101.
- 104 J. Y. Park, J. Gunpat, L. Liu, B. Edwards, A. Christie, X.-J. Xie, L. J. Kricka and R. P. Mason, *Luminescence*, 2014, **29**, 553–558.
- 105 J.-C. Tseng and A. L. Kung, *J. Biomed. Sci.*, 2015, **22**, 45.
- 106 N. Hananya, A. Eldar Boock, C. R. Bauer, R. Satchi-Fainaro and D. Shabat, *J. Am. Chem. Soc.*, 2016, **138**, 13438–13446.
- 107 J. Zalejski, J. Sun and A. Sharma, *J. Imaging*, 2023, **9**, 192.
- 108 F. Zheng, W. Xiong, S. Sun, P. Zhang and J. J. Zhu, *Nanophotonics*, 2019, **8**, 391–413.
- 109 T. Eilon-Shaffer, M. Roth-Konforti, A. Eldar-Boock, R. Satchi-Fainaro and D. Shabat, *Org. Biomol. Chem.*, 2018, **16**, 1708–1712.
- 110 L. J. van 't Veer and R. Bernards, *Nature*, 2008, **452**, 564–570.
- 111 R. N. Woodring, E. G. Gurysh, E. M. Bachelder and K. M. Ainslie, *ACS Appl. Bio Mater.*, 2023, **6**, 934–950.
- 112 M. I. Khan, M. I. Hossain, M. K. Hossain, M. H. K. Rubel, K. M. Hossain, A. M. U. B. Mahfuz and M. I. Anik, *ACS Appl. Bio Mater.*, 2022, **5**, 971–1012.
- 113 S. Gnaim, A. Scamparin, S. Das, R. Blau, R. Satchi-Fainaro and D. Shabat, *Angew. Chem., Int. Ed.*, 2018, **57**, 9033–9037.
- 114 L. Feng, Z. M. Liu, J. Hou, X. Lv, J. Ning, G. B. Ge, J. N. Cui and L. Yang, *Biosens. Bioelectron.*, 2015, **65**, 9–15.
- 115 S. F. Sousa, M. J. Ramos, C. Lim and P. A. Fernandes, *ACS Catal.*, 2015, **5**, 5877–5887.
- 116 C. Morisseau, *Int. J. Mol. Sci.*, 2022, **23**, 4870.
- 117 F. Wang, Y. Wang, J. Zhang, S. Zheng, B. Xie, S. Lu, J. Zhou, C. Wang, F. Wang, M. Jiang and X. Chen, *Sens. Actuators, B*, 2023, **375**, 132880.
- 118 X. Liu, S. Zeng, M. Zhang, M. Jiang, Y. S. Kafuti, P. Shangguan, Y. Yu, Q. Chen, J. Wang, X. Peng, J. Yoon and H. Li, *Chem. Commun.*, 2022, **58**, 11438–11441.
- 119 C. Weng, H. Yang, B. S. Loh, M. W. Wong and W. H. Ang, *J. Am. Chem. Soc.*, 2023, **145**, 6453–6461.
- 120 E. M. Williams, R. F. Little, A. M. Mowday, M. H. Rich, J. V. E. Chan-Hyams, J. N. Copp, J. B. Smaill, A. V. Patterson and D. F. Ackerley, *Biochem. J.*, 2015, **471**, 131–153.
- 121 D. Liu, T. N. Wanniarachchi, G. Jiang, G. Seabra, S. Cao, S. D. Bruner and Y. Ding, *RSC Chem. Biol.*, 2022, **3**, 436–446.
- 122 R. S. Boddu, O. Perumal and D. K. Biotechnol. Appl. Biochem., 2021, **68**, 1518–1530.
- 123 W. Wang, J. Cai, N.-K. Wong, M. Hong, J. Deng, L. Jin, Y. Ran, Y. Zhang, Y. Zhou and B.-O. Guan, *Analyst*, 2022, **147**, 1449–1456.





- 124 A. Chevalier, Y. Zhang, O. M. Khmour, J. B. Kaye and S. M. Hecht, *J. Am. Chem. Soc.*, 2016, **138**, 12009–12012.
- 125 S. A. Yoon, J. Chun, C. Kang and M. H. Lee, *ACS Appl. Bio Mater.*, 2021, **4**, 2052–2057.
- 126 W. Sun, M. Tong, G. Liu, X. Wang, N. Fan, X. Song, D. Yang and D. Zhang, *Results Chem.*, 2021, **3**, 100177.
- 127 R. Tannous, O. Shelef, S. Gutkin, M. David, T. Leirikh, L. Ge, Q. Jaber, Q. Zhou, P. Ma, M. Fridman, U. Spitz, K. N. Houk and D. Shabat, *ACS Cent. Sci.*, 2024, **10**, 28–42.
- 128 J. Sun, Z. Hu, R. Wang, S. Zhang and X. Zhang, *Anal. Chem.*, 2019, **91**, 1384–1390.
- 129 L. S. Ryan, J. Gerberich, J. Cao, W. An, B. A. Jenkins, R. P. Mason and A. R. Lippert, *ACS Sens.*, 2019, **4**, 1391–1398.
- 130 A. L. Pey, C. F. Megarity and D. J. Timson, *Biosci. Rep.*, 2019, **39**, DOI: [10.1042/BSR20191874](https://doi.org/10.1042/BSR20191874).
- 131 M. Faig, M. A. Bianchet, P. Talalay, S. Chen, S. Winski, D. Ross and L. M. Amzel, *Proc. Natl. Acad. Sci. U. S. A.*, 2000, **97**, 3177–3182.
- 132 S. R. Punganuru, H. R. Madala, V. Arutla, R. Zhang and K. S. Srivenugopal, *Sci. Rep.*, 2019, **9**, 8577.
- 133 S. Son, M. Won, O. Green, N. Hananya, A. Sharma, Y. Jeon, J. H. Kwak, J. L. Sessler, D. Shabat and J. S. Kim, *Angew. Chem., Int. Ed.*, 2019, **58**, 1739–1743.
- 134 S. R. Pinnell and G. R. Martin, *Proc. Natl. Acad. Sci. U. S. A.*, 1968, **61**, 708–716.
- 135 S. D. Vallet, M. Guérout, N. Belloy, M. Dauchez and S. Ricard-Blum, *ACS Omega*, 2019, **4**, 8495–8505.
- 136 T. Liburkin-Dan, S. Toledano and G. Neufeld, *Int. J. Mol. Sci.*, 2022, **23**, 6249.
- 137 L. Leung, D. Niculescu-Duvaz, D. Smithen, F. Lopes, C. Callens, R. McLeary, G. Saturno, L. Davies, M. Aljarah, M. Brown, L. Johnson, A. Zambon, T. Chambers, D. Ménard, N. Bayliss, R. Knight, L. Fish, R. Lawrence, M. Challinor, H. Tang, R. Marais and C. Springer, *J. Med. Chem.*, 2019, **62**, 5863–5884.
- 138 J. Huang, C. Zhang, X. Wang, X. Wei and K. Pu, *Angew. Chem., Int. Ed.*, 2023, **62**, e202303982.
- 139 R. J. Obaid, E. U. Mughal, N. Naeem, A. Sadiq, R. I. Alsantali, R. S. Jassas, Z. Moussa and S. A. Ahmed, *RSC Adv.*, 2021, **11**, 22159–22198.
- 140 T.-S. Chang, *Materials*, 2012, **5**, 1661–1685.
- 141 O. Shelef, A. C. Sedgwick, S. Pozzi, O. Green, R. Satchi-Fainaro, D. Shabat and J. L. Sessler, *Chem. Commun.*, 2021, **57**, 11386–11389.
- 142 M. H. Hanigan, in *Advances in Cancer Research*, ed. D. M. Townsend and K. D. Tew, Academic Press, 2014, vol. 122, pp. 103–141.
- 143 P. N. Brennan, J. F. Dillon and E. B. Tapper, *Liver Int.*, 2022, **42**, 9–15.
- 144 M. B. West, Y. Chen, S. Wickham, A. Heroux, K. Cahill, M. H. Hanigan and B. H. M. Mooers, *J. Biol. Chem.*, 2013, **288**, 31902–31913.
- 145 R. An, S. Wei, Z. Huang, F. Liu and D. Ye, *Anal. Chem.*, 2019, **91**, 13639–13646.

